Original Paper

Landslides (2023) 20:1115–1133
DOI 10.1007/s10346-023-02030-w
Received: 7 October 2022
Accepted: 31 January 2023
Published online: 17 February 2023

Yanqian Pei · Haijun Qiu · Yaru Zhu · Jiading Wang · Dongdong Yang · Bingzhe Tang · Fei Wang · Mingming Cao

Elevation dependence of landslide activity induced by climate change in the eastern Pamirs

Abstract The elevation dependence of climate change is unequivocal. Landslides (slides and debris flows) are the key mark of climate change acting on the land cryosphere, and they can pose a severe threat to the downslope or downstream community. However, whether there is an elevation dependence of landslide activity caused by climate change is unknown. In this study, Taxkorgan County in the eastern Pamirs was designated as the target area for studying the elevation dependence of shallow landslide activity. The volume and number of landslides have gradually increased over the last 20 years as the climate has become warmer and wetter. Small-sized ($< 50 \times 10^3$ m^3) slides induced by torrential rainfall are concentrated in areas below the 0 °C isotherm curve, while larger volume ($> 50 \times 10^3$ m^3) debris flows caused by the maximum temperature are distributed in areas above the 0 °C isotherm curve. Moreover, the landslides induced by climate change in the study area have a significant elevation dependence. In particular, the number and volume of debris flow affected by the maximum temperature in the areas above the 0 °C isotherm curve gradually increase with elevation. In the future (2020–2049), more small-sized slides will occur below the 0 °C isotherm curve as the climate continues to become warmer and wetter. The number and volume of the large-volume debris flow in the regions above the 0 °C isotherm curve will continuously increase with elevation. Our findings suggest that identifying and predicting the volume, number, and triggering factors of landslides within different elevation intervals should contribute to the more accurate assessment and management of landslide risks at the regional scale.

Keywords Landslides · Elevation dependence · Climate change · Eastern Pamirs

Introduction

The fact that the Earth's climate system is warming and that this warming is amplified at high elevations is unequivocal (Pepin et al. 2015; Yao et al. 2016), and the fact that climate change affects the stability of natural and engineered slopes and impacts landslides is also undisputable (Shi and Xu 2008; Ohmura 2012; Haeberli and Whiteman 2015). The variations in the size, number, and inducing factors of landslides at high elevations are due to global warming (Hock et al. 2019).

A landslide is a mass movement erosion process acting on natural and engineered slopes. They occur worldwide and play an important role in geomorphic evolution. Landslides can be triggered by various mechanisms, including precipitation, snowmelt, temperature changes, seismic shaking, volcanic activity, and various human activities (Allen et al. 2016; Zaginaev et al. 2016). In the high mountains in Asia, which are characterized by low precipitation, sparse vegetation, and fragile ecosystems, landslides have exhibited accelerated expansion with global warming and pose a serious threat to downslope or downstream communities and infrastructure (Petley 2012; Li et al. 2016a, b; Wirz et al. 2016; Chai et al. 2018; Eriksen et al. 2018; Jiang et al. 2021; Zhou et al. 2022; Qiu et al. 2022). However, our understanding of the specific impacts of climate change on the type, size, frequency, and activity of landslides within different elevation intervals remains poor (Hewitt 2009; Fujita et al. 2013; Harrison et al. 2018; Hock et al. 2019; Veh et al. 2020). Quantifying the relationships between landslides and climate change within different elevation regions requires long-time series landslide inventories and a set of meteorological data (Guzzetti et al. 2012; Piacentini et al. 2018; Tanyaş et al. 2017; Rossi et al. 2010), which is often missing for (remote) high elevation mountains (Key et al. 1997; Zhang et al. 2012; Miralles et al. 2014; Jiang et al. 2016; Schulz et al. 2008). This has resulted in studies of landslides in alpine regions typically focusing on methods of assessing the impact of climate change on landslides and the effect of climate (and its change) on slope stability (Cody et al. 2020), such as the use of downscaled climate predictions to assess slope stability conditions (Coe 2012), analysis of paleo-landslide events and climate records (Coe and Godt 2012; Coe et al. 2018), and qualitative analysis of individual slope/landslide stability (Schneider 2004; Jiang et al. 2021).

To gain a better understanding of how the degradation of the cryosphere with climate change affects the development of landslides in alpine regions, we used a historical landslide inventory and a set of climatic data that can reflect climate change in (remote) high mountain regions to quantify the landslide-climate relationship within different elevation intervals and to predict the hazards and risks posed by future climate change-induced landslides in the corresponding zones.

Study area

Overview of Taxkorgan County

We selected Taxkorgan County in the eastern Pamirs as the study area to study the elevation dependence of landslide activity and climate change (Fig. 1a). This region (Pamirs and Karakorum) is one of the five bellwether sites for world landslides proposed by Coe (2020), in which landslides respond the most sensitively to climate change (Fig. 1b). We used archival records, remote sensing interpretation, and field investigations to map a total of 258 landslides (142 slides and 116 debris flows) with individual areas of greater than 0.5 km^2 in the region over the last 20 years (Figs. 2, 3, 4, and 5).

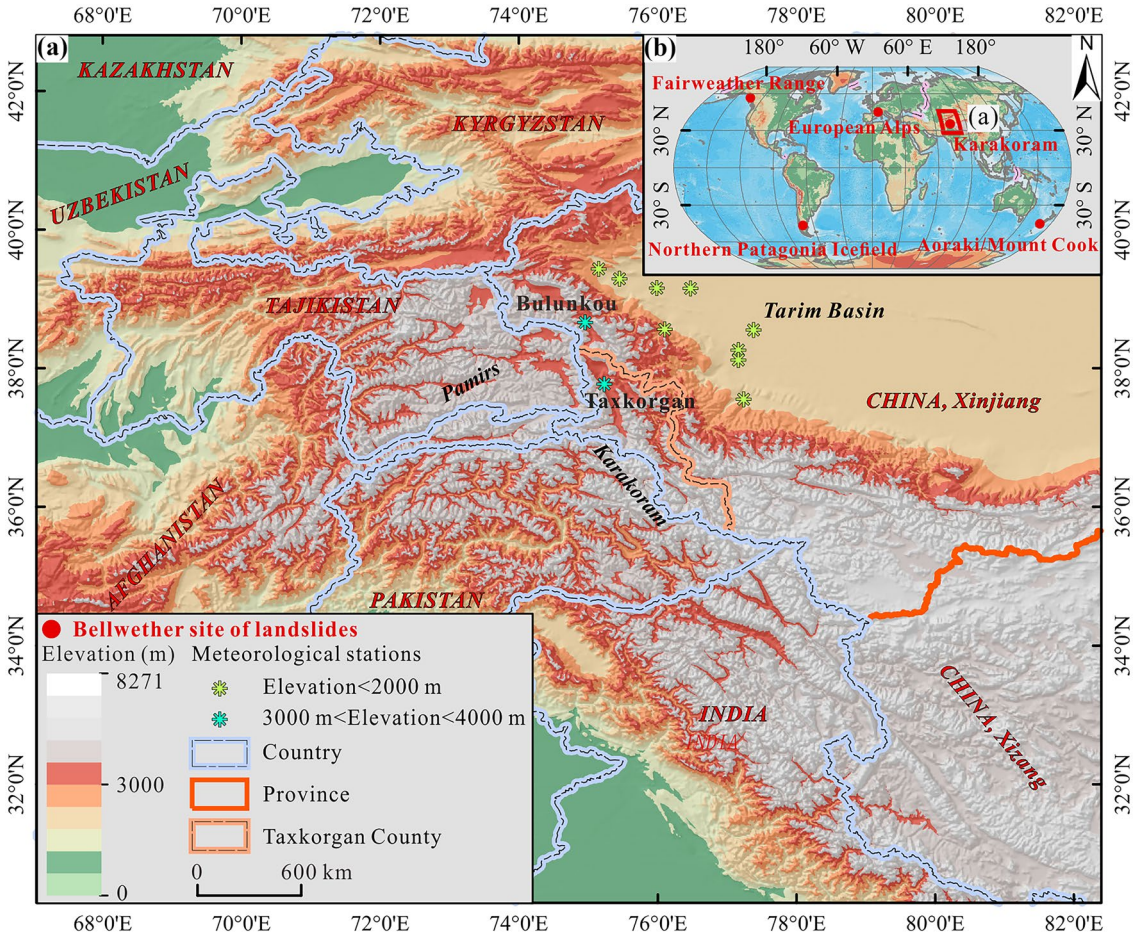

Fig. 1 Overview of Taxkorgan County. **a** Location of Taxkorgan County. The meteorological stations are operated by the meteorological department. **b** The five landslide bellwether sites with high sensitivity to climate change worldwide (Coe 2020)

Topography and landslides

The relief of this region is rugged (elevation of 1773–8538 m), with an average elevation of 4000 m (Fig. 2). The area above 4000 m in the study area accounts for 64.3% of the total area, and 83.5% of the large-sized debris flows and 72% of the small-sized slides occurred in the areas with elevations of greater than and less than 4000 m, respectively. We extracted the 0 °C isotherms for the warm season (April–October) in the study area in 2000, 2010, and 2019 based on downscaled air temperature data that consider the influence of topographic factors (digital elevation model, DEM) on the temperature field (Fig. 2). It was found that the elevation of the 0 °C isotherm curve in the study area has increased by 186.38 m since 2000, and the average elevation of the 0 °C isotherm curve is 4061.196 m over past 20 years (2000–2019).

Geologic setting and landslides

In Taxkorgan County, the geological conditions are complex, and the tectonics are active (Fig. 3). The lithology mainly includes Ordovician (siliceous rocks), Cretaceous (grayish-green mudstone), Quaternary (gravel), Permian (andesite, carbonaceous siltstone, siltstone, granite), Variscan Devonian (diorite), Variscan Carboniferous (diorite, granite, moyite), Silurian (moyite, slate), Triassic (conglomerate), Carboniferous (limestone), Proterozoic (carbonate rocks, metamorphic sandstone), Yanshan (moyite, granodiorite), Indosinian (granite, granodiorite), Mesoproterozoic (granodiorite, diorite), and Jurassic (siltstone) strata. The fault system consists of active faults, thrust faults, normal faults, strike-slip faults, and suture zones. These faults provide favorable conditions for landslides.

Landform characteristics, groundwater, and landslides

The landform types in Taxkorgan County, located in the Pamirs and Karakoram, include glacial erosion (eroded by glaciers) and denudation (weathering in alpine areas) landforms in the alpine areas; erosion-denudation (flow erosion and weathering) landforms in the mid-alpine areas; and alluvial plains, accumulation plains (ice and water), and moraine dams in the valleys (Fig. 4). The study area is dominated by glacial erosion, denudation, and erosion-denudation

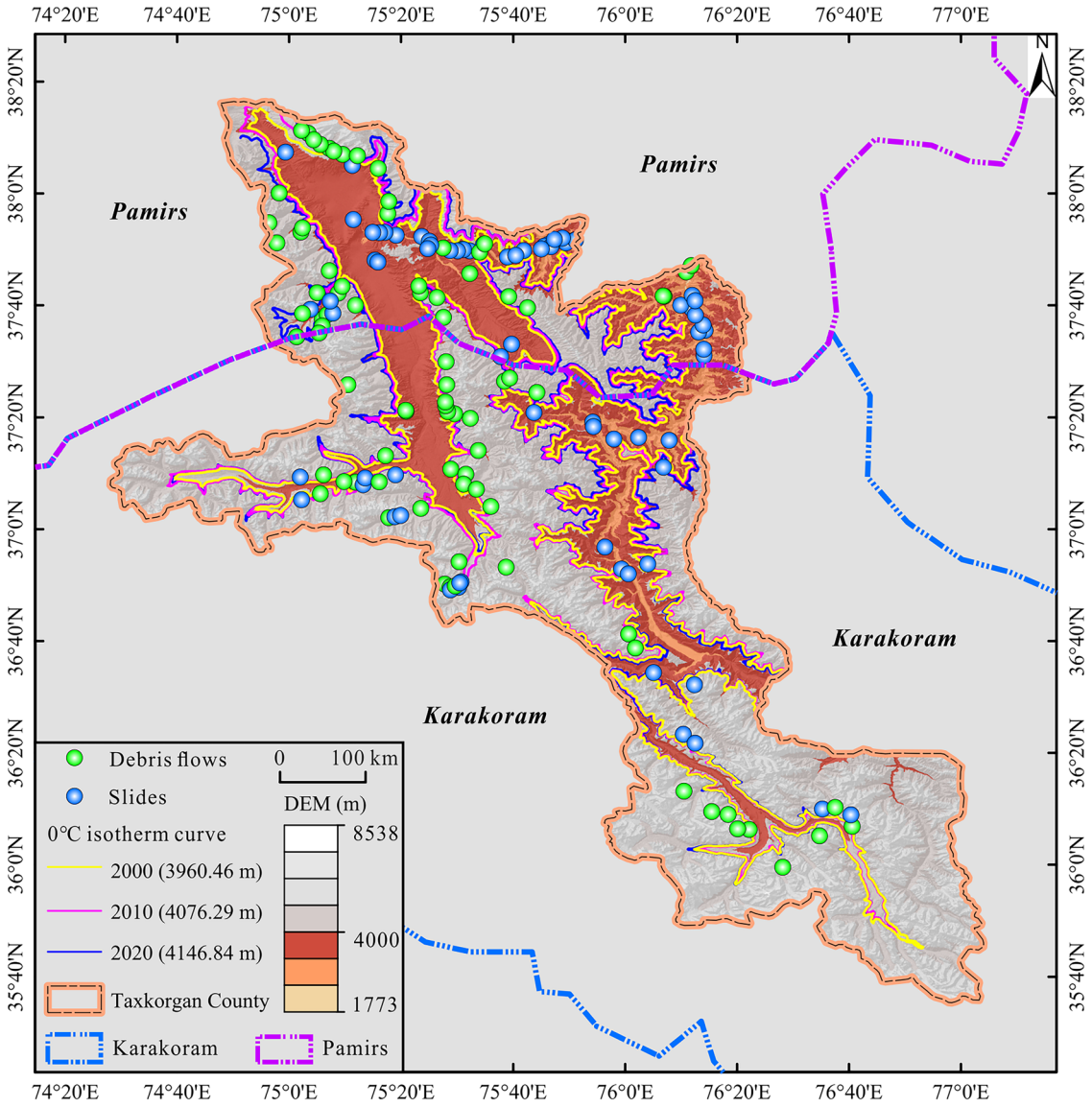

Fig. 2 Topography of Taxkorgan County, 0 °C isotherm curve, and distribution of the slides and debris flows. The 0 °C isotherm curves were extracted from downscaled temperature data that consider the influence of topographic factors (DEM) on the temperature field. The boundaries of the Pamirs and Karakoram are revised by Zhang et al. (2022)

landforms, which account for 89.3% of the total area of the study area. Moreover, 90.6% of the debris flows are distributed in the glacial erosion and erosion-denudation landforms; while most of the slides (92%) are distributed in the erosion-denuded landforms and alluvial valley plains.

In Taxkorgan County, which is located in an alpine arid-semi-arid climate zone, glaciers, and permafrost are widely distributed, and groundwater is relatively scarce (Fig. 5). Overall, 89.3% of the study area contains glaciers, permafrost, and/or clastic rock (fissure-pore water = 0.1–1L/S; 2–20m^3/d.m) and stratified and metamorphic rock (fissure water > 1L/S; > 20m^3/d.m). Statistically, 79% of the debris flows and 83% of the slides are located in these areas.

Materials and methods

Landslide inventory

Landslide data

With global warming, landslides induced by snow melt, glacier retreat, and permafrost degradation are common in Taxkorgan County. Figure 6 shows typical landslides within different elevation intervals in the study area. Landslides, unlike other natural processes, are not typically monitored by devices (Rossi et al. 2010; Liu et al. 2021, 2022; Ma et al. 2023; Wang et al. 2022). As a result,

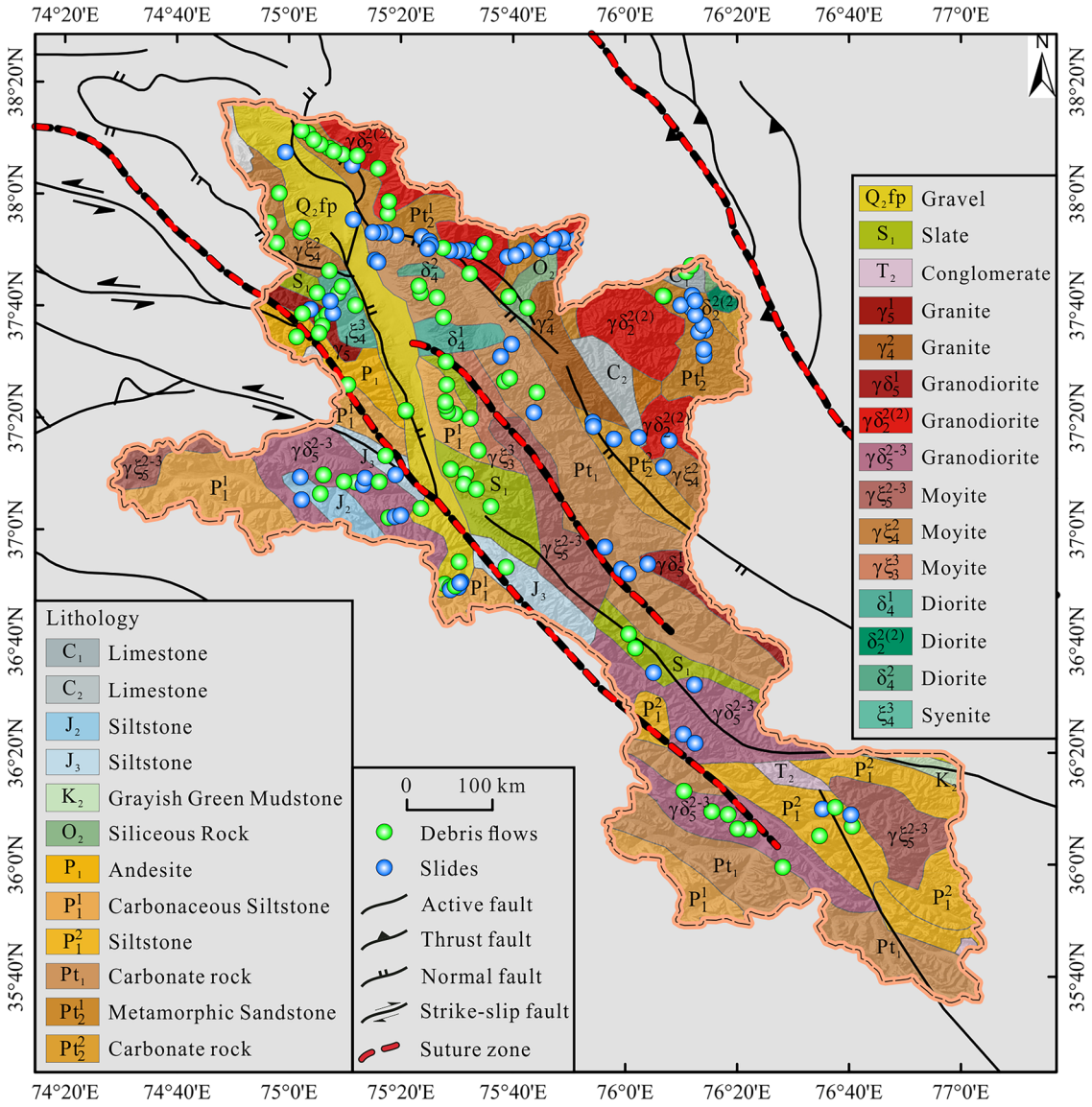

Fig. 3 Geological overview. The lithology is derived from the Geographic Data Sharing Infrastructure, College of Urban and Environmental Science, Peking University (https://geodata.pku.edu.cn/index.php?c=content&a=show&id=709). The faults are modified from Robinson et al. (2007)

compiling a consistent and comprehensive list of historical landslides is challenging (Guzzetti et al. 2000; Rossi et al. 2010; Zhang et al. 2012; Jiang et al. 2016). By examining the Geological Disaster Prevention Yearbook released by the Taxkorgan County administration, newspapers, literature (Coe 2020; Yuan et al. 2013), scientific reports, and historical archives, we created a list of historical non-earthquake, non-anthropogenic landslides, and a landslide time series. The Yearbook lists the landslides' geographic location, type, date of occurrence, volume, and depth, as well as the financial losses and fatalities they caused.

The strength of the Yearbook is its authority and reliability. Under the current disaster assistance system in China, government department offices are mandated to notify their parent department of each landslide event. The landslide information in the Yearbook is collected and compiled by the Natural Resources Bureau of Taxkorgan County. It is finally submitted to the Taxkorgan County government in the form of a Detailed Geological Hazard Report for publication in the Taxkorgan County Disaster Prevention and Control Yearbook. Local administrators usually assess the effect of landslides using the yearbook's inventory and implement the necessary prevention and control measures for significant landslides. However, the Yearbook still has shortcomings, such as data completeness. When a disaster occurs, the local government authorities give priority to collecting information about disasters that affect infrastructure, cause casualties, and are located near roads, villages, or towns. As a result, a comprehensive list of landslides over a lengthy period is unavailable because the Yearbook does not cover every landslide that took place in the relevant area during the relevant time period. However, a relatively complete landslide inventory is meaningful and necessary for

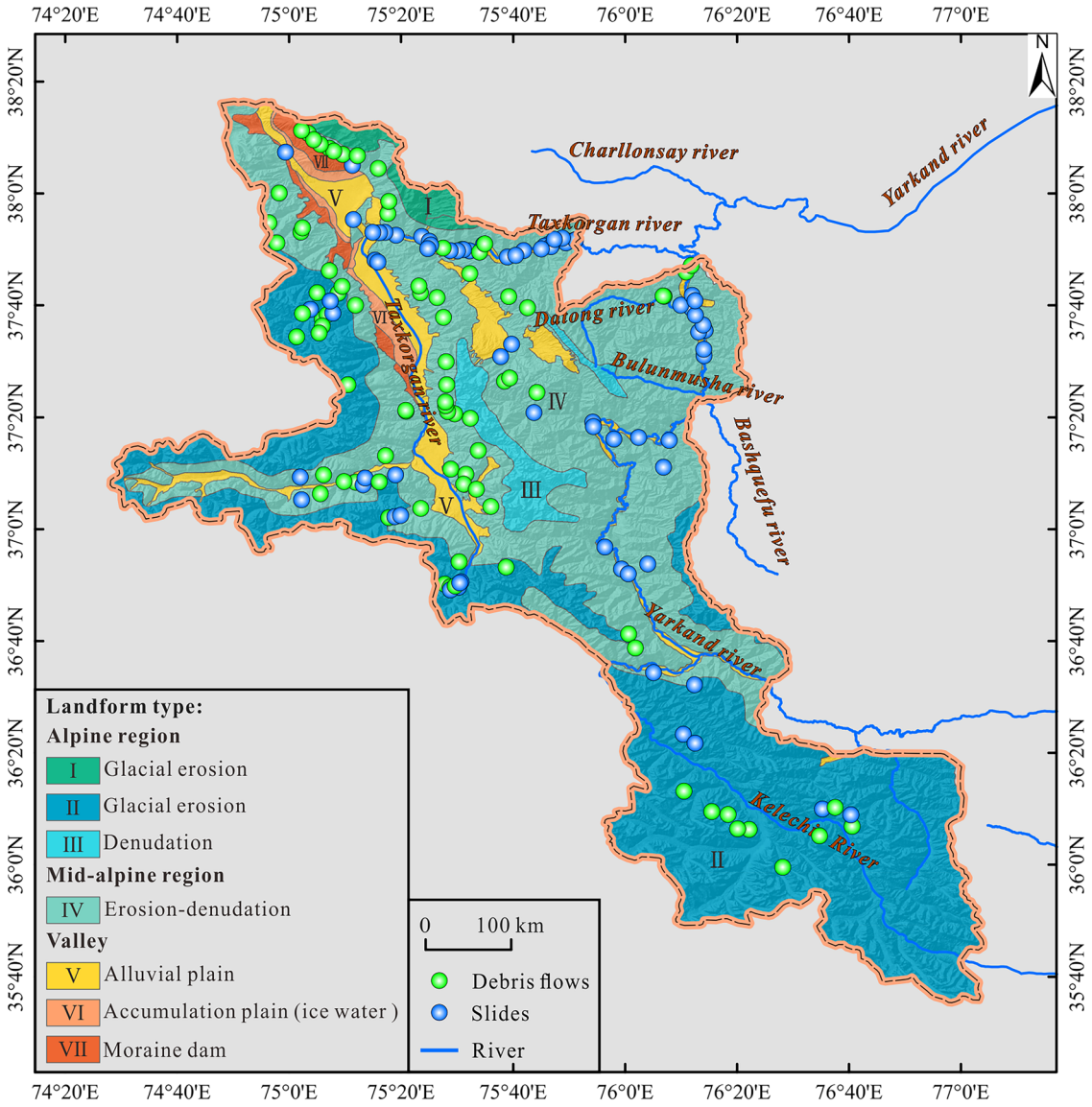

Fig. 4 The landform types (modified from Ma et al. (2016))

disaster prevention and landslide research. A sufficiently complete landslide inventory can reflect the relationship between landslides and climate change well and reveal its impact on landscape evolution and human life (Kirschbaum et al. 2010; Petley 2012).

The common tools for reconstructing a relatively complete landslide inventory, especially for identifying historical landslides, are remote sensing interpretation and field surveys. Carrara et al. (2003) state that determining the date of historical landslides using remote sensing images is difficult for geoscientists. In particular, vegetation changes can obscure landslide boundary changes. However, the vegetation in Taxkorgan County, which is located in the alpine climate zone, is scarce all year round, which greatly reduced the influence of vegetation changes on the landslide boundaries during our interpretation. In this study, we collected a total of 869 optical images (Landsat 8 and ASTER) of the study area with less than 20% cloud cover for the last 20 years (2000–2019), and then, we conducted comparison and visual interpretation to verify the occurrence date and location of 172 landslides in the Yearbook and to interpret landslides that occurred in other locations at the same or a different time as those in the Yearbook. Finally, we reconstructed a landslide catalog consisting of 258 landslide events with individual areas of greater than 0.5 km^2. Based on the landslide classification proposed by Cruden and Varnes (1996) and the modifications to the landslide classification system proposed by Hungr et al. (2014), the reconstructed landslide catalog included 142 slides and 116 debris flows. However, we do not distinguish the initial materials (rock, soil, colluvium, or both) of slides and debris flows. The volume of the slide was less than 82.9×10^3 m^3, and the volume of the debris flow ranged between 24.56×10^3 and 739.7×10^3 m^3. The slide depths range between 0.3 and 5 m, and the depth of only one slide is 8 m. The debris flow fan thicknesses range between 0.03 and 1 m. Therefore, all the landslides in this paper are shallow landslides.

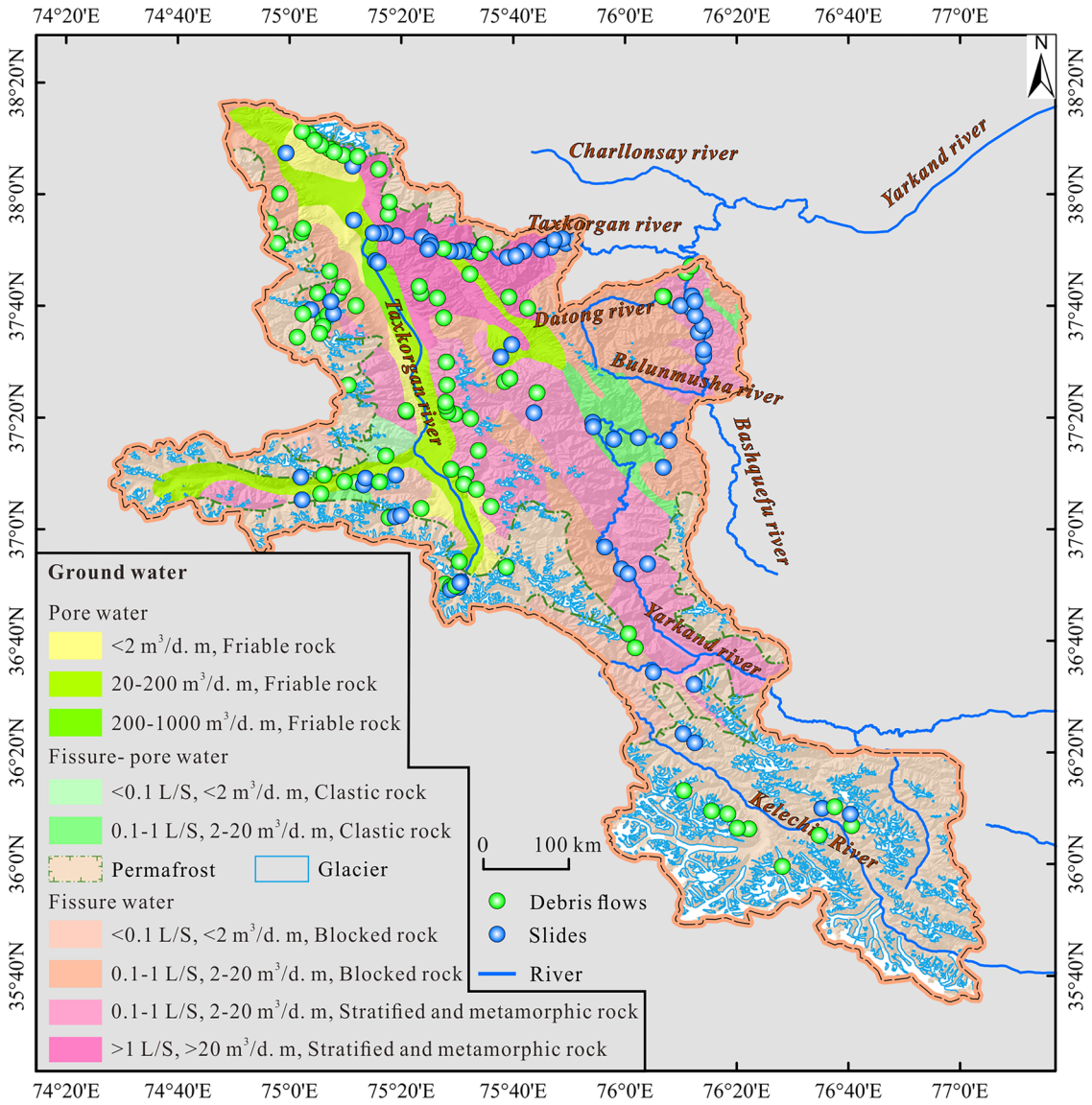

Fig. 5 Hydrological map. The groundwater distribution is modified by Ma et al. (2016). The glaciers were obtained from the Randolph Glacier Inventory (RGI V6.0) (Zhang et al. 2015; Rgi and Nosenko 2017)

The attribute sheet of the catalog also includes the number, type, geographic location, date of occurrence, volume, depth, and threat objects (e.g., settlements, houses, roads, hydropower stations, and power facilities) of each landslide event. For the reconstructed landslide catalog, we conducted field investigations to verify them in 2021. For the 86 new landslides (49 slides and 37 debris flows), the boundaries were verified using aerial photographs and orthophotos taken by an Unmanned Aerial Vehicle (UAV), and the occurrence date of each landslide was confirmed using questionnaires and interviews. Notably, questionnaires were completed and interviews were conducted with local geohazard practitioners who had participated in disaster prevention and relief and with local herders who had some knowledge of the landslides.

Volume of the interpreted landslide

In this study, the deposition areas of most of the debris flows were mainly fan-shaped (Fig. 7a). To accurately calculate the volumes of debris flows, mathematical models were built based on the geometric characteristics of their deposition areas, and the total material volume was estimated using a DEM. Notably, we only calculated the volume of one event with the largest change in the deposition fan boundary in the last 20 years. The following formula can be used to determine the volumes of the debris flows:

$$V_D = \frac{1}{6}L^2h(\alpha - \sin\ \alpha), \tag{1}$$

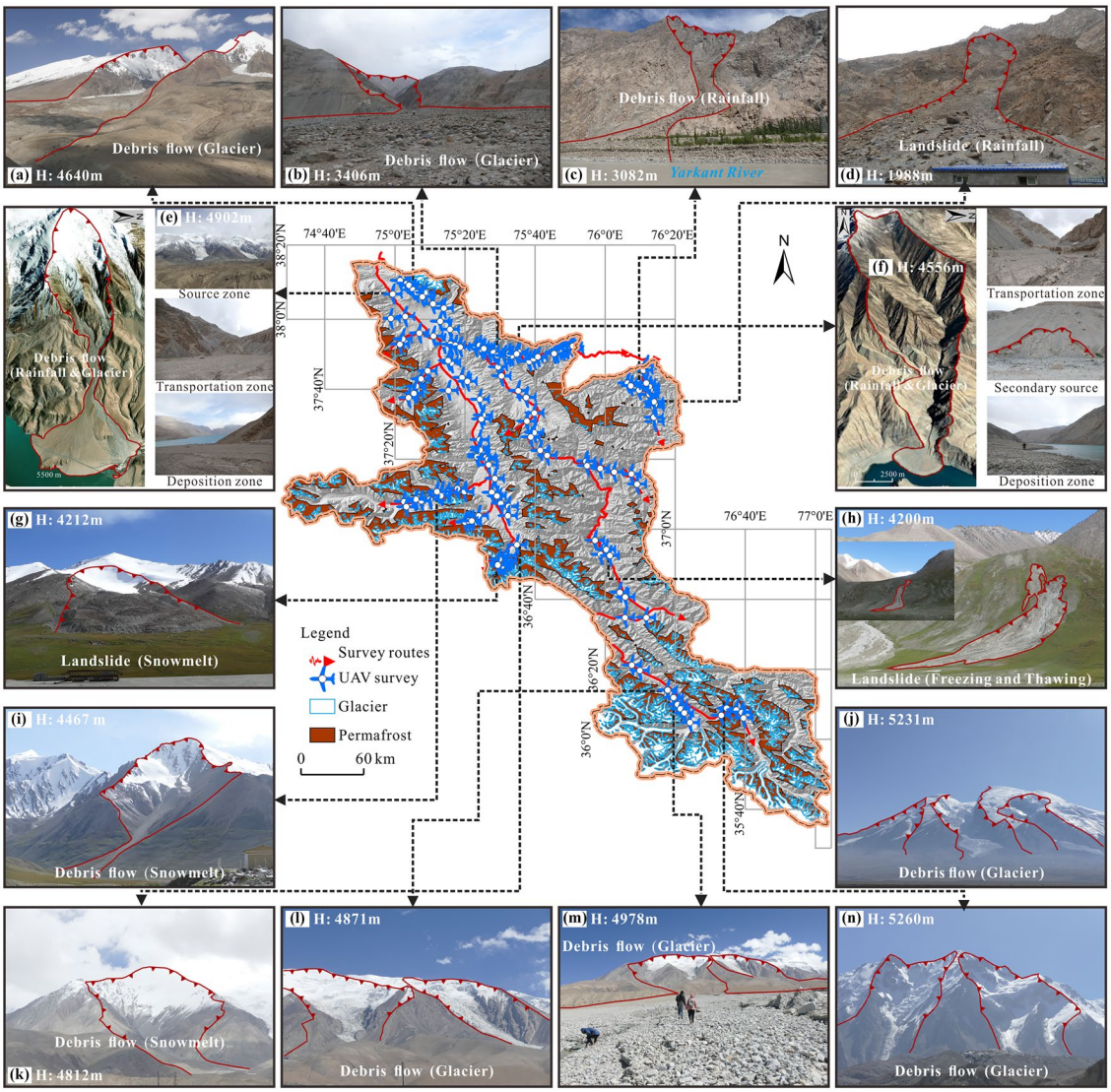

Fig. 6 Overview of the landslide sites visited in Taxkorgan County. The photos and images were acquired using a UAV (DJI Mavic 2 pro) during the field surveys in September 2019 and August 2021. **a–n** show the types and triggering factors of the landslides within the different elevation intervals

where V is the potential volume of the debris flows (m^3), L is the length of the fan (m), h is the thickness of the fan (m), and α is the angle of the debris slide (°).

Figure 7b depicts the empirical relationship between the volume and area of the slides based on data for 172 landslides documented in the Yearbook.

Based on information for 172 landslides listed in the yearbook, the empirical link between the volume and area of the slides is illustrated in Fig. 7b. According to Fig. 7b, there is a clear linear relationship between the volume and area of the slides with various orders of magnitude in log–log coordinates. This results in the following relationship:

$$\log(V_s) = 0.87 \log A_s + 0.59 \ (R^2 = 0.94,\ p << 0.01), \quad (2)$$

where V_S is the volume of slides and A_S is the area of slides.

Finally, we selected two empirical links to establish the bounds of the slide volume and to quantify the uncertainty of this empirical formula. The upper and lower 95% prediction ranges are displayed in Fig. 7b.

Meteorological data

In alpine regions where there is no meteorological observation equipment, it has become common practice to use reanalysis data and satellite-reproduced data to study regional climate change (Khadka et al. 2014; Nie et al. 2017; Kirschbaum et al. 2020; Ni et al. 2020). In this study, to obtain climate data that reflect the climate change in the study area, we downscaled the Global Land Data Assimilation System Dataset (GLDAS) based on observations from

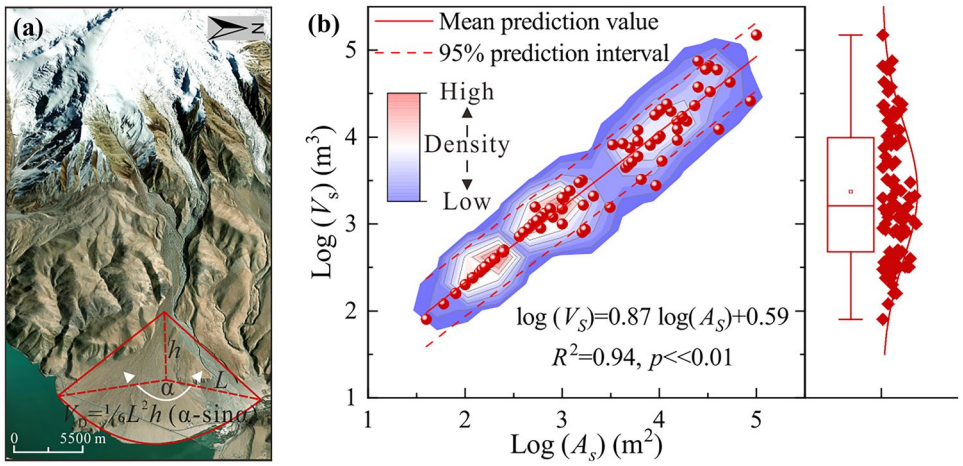

Fig. 7 Volume of the interpreted landslides. **a** The volume of the interpreted debris flows (Zou et al. 2020). **b** The empirical relationship between the slide volume and area. The linear least-squares method yielded the best fit, which is denoted by the thick red line. The dashed red lines represent the 95% confidence intervals. The contours depict the bivariate kernel density estimation point density. The box plot displays the descriptive statistics about the volume of the slides in the Yearbook

ten meteorological stations (elevations of < 2000 m) (Fig. 1a). The downscaled meteorological data were calibrated to the elevation using the vertical decline rates of the temperature (0.57°C/100 m) (Kang et al. 2022), and the precipitation (daily max, mean, and min) and temperature (daily max, mean, and min) data had a resolution of 1 km. Notably, the precipitation distribution in the region was not uniform, and the annual precipitation and the days with > 24 mm of precipitation did not represent the mean precipitation in the entire region, but rather the precipitation in the alpine regions. Torrential rainfall was defined as more than 24 mm of precipitation in 24 h in Xinjiang, China (Yao et al. 2022). The number of torrential rainfall days and the maximum temperature are abbreviated in this paper as R_{24} and T_{max}, respectively. GLDAS data with temporal and spatial resolutions of 3 h and 0.25° × 0.25° have been widely used globally and have high reliability (Liu et al. 2019; Deng et al. 2020; Qi et al. 2020). We validated the downscaled data using observations from two meteorological stations (Fig. 1a) located in the higher elevation region (3000–4000 m) and WorldClim V2.1 data (Panagos et al. 2017). For the observations, we created a 1 km buffer for the meteorological stations in the horizontal and vertical directions, respectively, and extracted the downscaled data inside the buffer for comparison with the observations. For the WorldClim V2.1 data, we verified the accuracy of the downscaled data according to the trend of climate change. Although there was some error (± 0.2 °C) between our downscaled meteorological data and the station observations, our data were generally consistent with the WorldClim V2.1 data. The accuracy of our data in the vertical direction was higher than that of the WorldClim V2.1 data, and thus, our data can more accurately reflect climate change in high-elevation regions.

The delta downscaling method is the primary generation technique for future climatic scenarios recommended by the US National Assessment and is simple and commonly used (Diaz-Nieto and Wilby 2005; Hay et al. 2010). However, it ignores the elevation dependence of temperature and precipitation (Rolland 2003; Firozjaei et al. 2020). In this study, we developed a downscaling method (i.e., the revised delta downscaling method) for low-resolution meteorological data, which takes into account the temporal and spatial (elevation) trends of the climate data. We used the vertical decline rates of the temperature to appraise the error in the meteorological data generated by the downscaling method. The vertical decline rates of the temperature remained at 0.6 ± 0.2 °C, which is consistent with the results of most studies (Liu et al. 2019; Deng et al. 2020; Fatolazadeh et al. 2020; Qi et al. 2020). The equations of the revised delta downscaling method are as follows:

$$P = P_0 f\left(Spatial\ trend, Verticalvariation\right) + \delta, \tag{3}$$

$$T = \left[T_0 f\left(Spatialtrend, Verticalvariation\right) + \delta\right] + \Delta H\gamma, \tag{4}$$

where P (mm) and T (°C) are the precipitation and temperature after downscaling, respectively; and P_0 (mm) and T_0 (°C) are the precipitation and temperature of the GLDAS data, respectively. The spatial trend is the horizontal trend, i.e., the interpolated result of the observations at the meteorological stations; and the vertical variation is the vertical trend, i.e., the interpolated result of the observations at different elevations. δ is the deviation correction; γ is the temperature lapse rate (0.57 °C/100 m), and ΔH is the vertical deviation correction of the temperature (m). The downscaling process was carried out using Python software.

For the future conditions, we simulated the monthly temperature and precipitation (rainfall and snowfall) data with of resolution of 1 km from 2020 to 2100 for the study area under three shared socioeconomic pathways (SSP2.6, SSP4.5, and SSP8.5) using 27 climate models from the Intergovernmental Panel on Climate Change (IPCC) Sixth Assessment Report (Grose et al. 2020; Kirschbaum et al. 2020), based on the WorldClim version V2.1 dataset and the revised delta downscaling method, to discuss the elevation dependence of landslide activity induced by future climate change. Phase 6 of the Coupled Model Intercomparison Project (CMIP6) uses a matrix framework of shared socioeconomic pathways (SSPs) and representative concentration pathways (RCPs), which has a better resolution compared to CMIP5 (Ma et al. 2020; Grose et al. 2020; Hu et al. 2021).

Results

Landslides and climate trend characteristics

Based on past climate changes and the availability of landslide data, we analyzed the changes in the climate and landslides in this region over the past 20 years (2000–2019) (Fig. 8). It was found that the

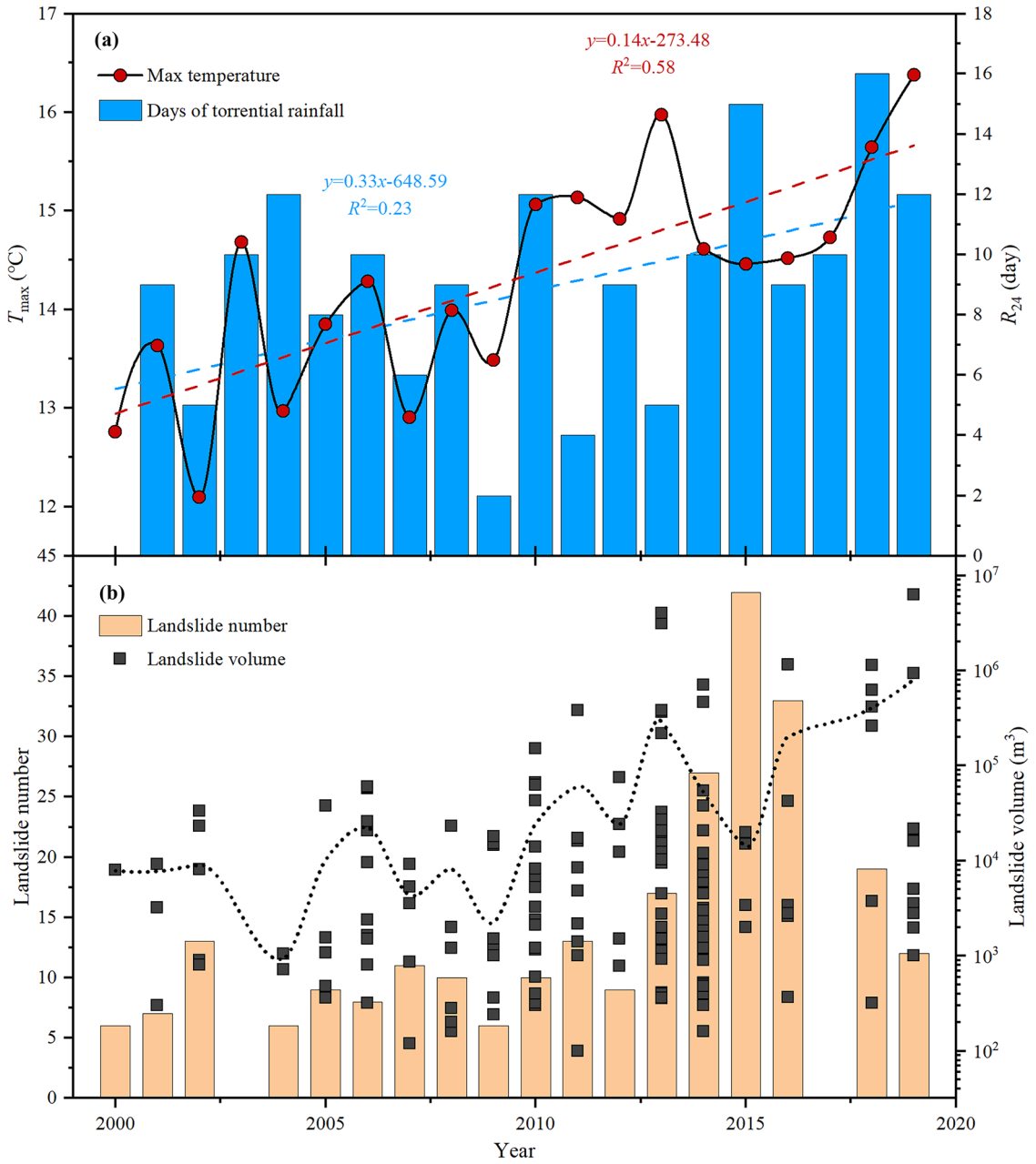

Fig. 8 Climate change and landslide distribution in Taxkorgan County over the past 20 years. The black dashed line is the landslide volume fitted with a LOESS function (Jakob and Owen 2021)

climate in the study area has exhibited a more pronounced warming and wetting trend since 2000. This is supported by a significant increase in the T_{max} (1.4 °C/10a) and an increase in the number of days of torrential rainfall (3.3 days/10a) (Fig. 8a). The volume and number of landslides are also gradually increasing (Fig. 8b). According to the locally estimated scatter smoothing (LOESS) function curve (Jakob and Owen 2021), the landslide volume is increasing by 24,606 m³ per decade, indicating a significant increasing trend at the 99% significance level.

Evidence of elevation-dependent warming and wetting

We divided the study area into nine elevation intervals using the natural section point method in ArcGIS. We discovered that 74% of the area of Taxkorgan County has an elevation of 2500–5000 m, while the areas of the county with an elevation of fewer than 2500 m and an elevation greater than 5000 m are relatively small, accounting for only 26% and 8.1% of the study area's total area, respectively. To investigate the elevation dependence of landslides

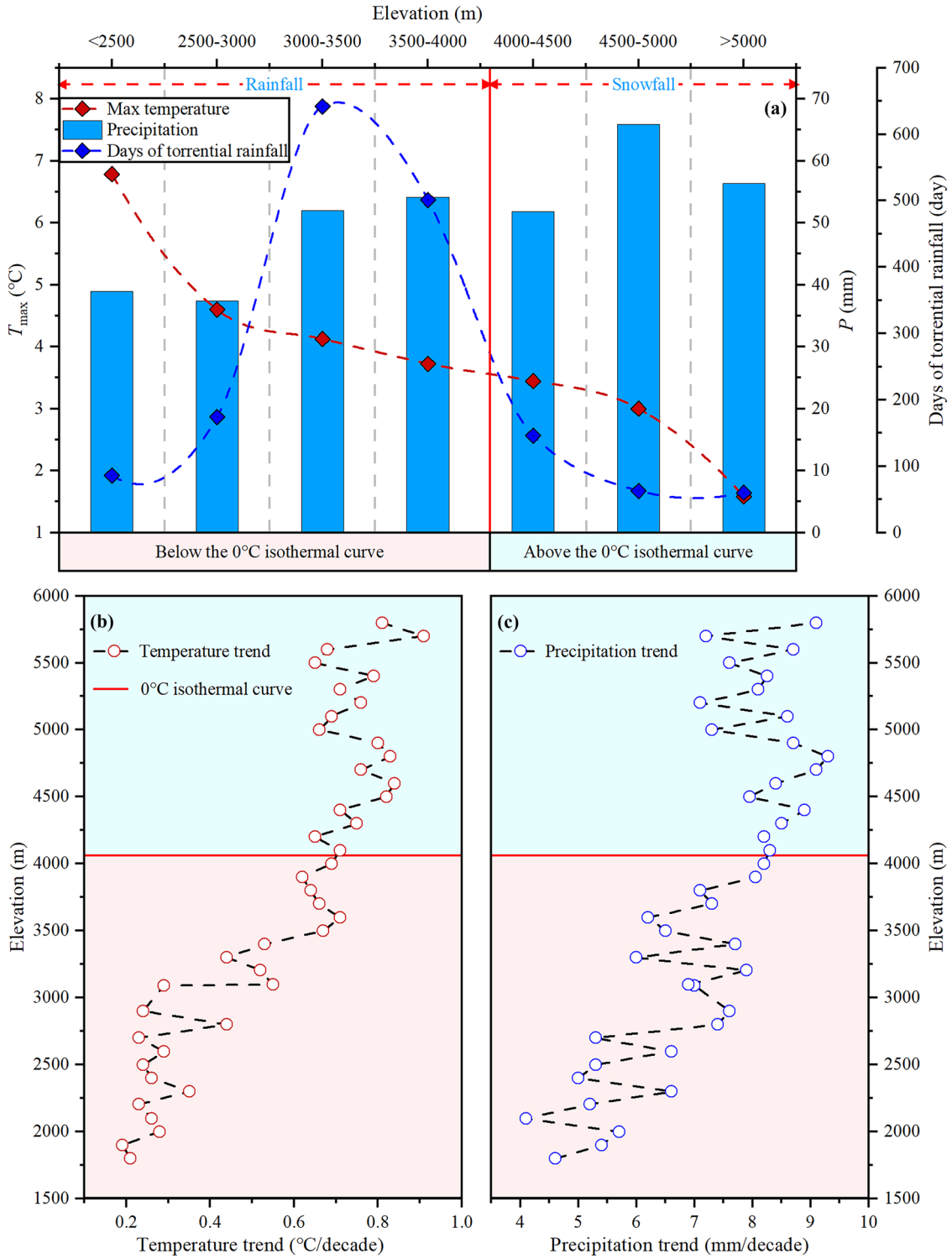

Fig. 9 Climate change within the different elevation intervals. **a** Distributions of the maximum temperature, precipitation, and torrential rainfall. **b** Temperature trends within the different elevation intervals. **c** Precipitation trends within the different elevation intervals. Notably, the number of days of torrential rainfall refers to the number of days with a 24-h rainfall of greater than 24 mm within the different elevation intervals over the past 20 years. The red circles represent the warming rate (temperature trend) of the maximum temperature over the past 20 years (2000–2019) at different elevations. The blue circles represent the rate of increase (precipitation trend) of precipitation over the past 20 years (2000–2019) at different elevations

caused by climate change in this area, we separated the region where the elevation is between 2500 and 5000 m into five 500-m intervals, as well as two intervals with elevations of less than 2500 m and more than 5000 m.

The distributions of the T_{max}, precipitation (rainfall and snowfall), and the number of days of torrential rainfall in Taxkorgan County within the different elevation intervals are depicted in Fig. 9a. During the past 20 years (2000–2019), the cumulative precipitation was positively correlated with elevation, T_{max} was inversely correlated with elevation, and the torrential rainfall was greatest between elevations of 2000 and 4000 m. Notably, 84% of the torrential rainfall occurred in the regions below the 0 °C isotherm curve; and although there was a great deal of precipitation in the areas above the 0 °C isotherm curve, the number of days of torrential rainfall was very small. The lower temperatures above the 0 °C isotherm curve caused the majority of the precipitation to all fall as snow in the areas above the isotherm. We only counted the number of days of torrential rainfall because snowfall does not induce landslides or debris flows. The temperature and precipitation trends within the different elevation intervals in the study area over the past 20 years are shown in Fig. 9b, c. Both the temperature trend and the precipitation trend in the study area exhibited a large elevation dependence, which means that both the temperature trend and the precipitation trend increased with elevation, and the elevation dependence was stronger in the region above the 0 °C isotherm curve. These results are consistent with the results of previous studies (Pepin et al. 2015; Yao et al. 2016, 2022; Pei et al. 2023).

Distribution of landslides with elevation

Figure 10 shows the distributions of the number and volume of the landslides within the different elevation intervals. As can be seen from Fig. 10, the number of slides and debris flows both initially increased and then decreased with elevation. The maximum number of slides occurred in the 3000–3500 m intervals, while the maximum number of debris flows occurred in the 4500–5000 m interval. The majority of the slides (88%) occurred in the area below the 0 °C isotherm curve, and the volume was relatively small. Only 12% of the large-volume slides occur in the intervals above the 0 °C isotherm curve, and their volume gradually increased with elevation. In contrast, a significant portion (75%) of the large-volume debris flows occurred in the intervals above the 0 °C isotherm curve, and the volume of these debris flows gradually increased with elevation.

Landslides with climate change-elevation relationship

The relationships between the number and volume of the landslides and the temperature trend in the area below the 0 °C isotherm curve are depicted in Fig. 11a, c. As can be seen from Fig. 11a, c, in the area below the 0 °C isotherm curve, the number and volume of slides both exhibited negative correlations with temperature, while the number of debris flows exhibited a positive correlation with temperature and the volume of the debris flows exhibited a positive exponential correlation with temperature (Fig. 11c).

Figure 11b, d depicts the relationships between the number and volume of the landslides and temperature above the 0 °C isotherm curve. It can be seen that the number of debris flows exhibited a significant positive correlation ($p < 0.5$) with temperature, and the volume of the debris flow exhibited a significant positive exponential relationship ($p < 0.5$) with temperature. The number of slides gradually decreased with temperature, while the volume of the slides exhibited a non-significant exponential correlation with the temperature. This indicates that the large-sized debris flows in the region above the 0 °C isotherm curve were mainly driven by the T_{max} and exhibited a strong elevation dependence, i.e., the number and volume of the debris flows increased with elevation during the 20-year period of record.

Figure 12a, c depicts the relationships between the number and volume of the landslides and the number of days of torrential rainfall in the areas below the 0 °C isotherm curve. The number and volume of the slides showed significant positive correlations ($p < 0.5$) and the volume of the slides showed a positive exponential relationship with the number of days of torrential rainfall; whereas, the number and volume of the debris flow had a negative correlation and a negative exponential relationship with the number of days of torrential rainfall, indicating that the torrential rainfall had a greater influence on the slides in the region below the 0 °C isotherm curve. Figure 12b, d shows the relationships between the number and volume of the landslides and the number of days of torrential rainfall in the region above the 0 °C isotherm curve. The number of days of torrential rainfall showed a negative correlation and a negative exponential relationship with the number and volume of the debris flows, while the volume of only a few slides showed a positive exponential link with the number of days of torrential rainfall. This indicates that in the areas above the 0 °C isotherm curve, the effect of the torrential rainfalls on the slides and debris flows was rather minimal.

Anticipation of futureclimate change

Figure 13 shows how the temperature, precipitation, and snowfall, which can cause landslides, will change in the future within the different elevation intervals under the SSP2.6, SSP4.5, and SSP8.5 scenarios. Regardless of the scenario, the maps in Fig. 13a–c show that the climate of the region will continue to warm in the future, resulting in a positive temperature trend. In contrast, only scenario SSP2.6 predicts a steady temperature increase between 2020 and 2100, with an increase in temperature with elevation. The temperature trend under scenario SSP4.5 decreases from 2050 to 2079, but it progressively increases with elevation. By 2080, the temperature trend will be higher, but it will be lower than that in 2050. The temperature trend will gradually increase from 2020 to 2079 under scenario SSP8.5, will peak during 2050–2079, and then will begin to decrease. However, the temperature trend will decrease with elevation.

Figure 13d–i shows the predicted future precipitation (rainfall and snowfall) in the study area. According to Fig. 13d–f, the rainfall trend will be positive from 2020 to 2049, and the area below the 0 °C isotherm curve will only become wetter under scenario SSP2.6. This suggests that at this time, the number of days of torrential rainfall in this area will increase. After this, it demonstrates that in the area below the 0 °C isotherm curve,

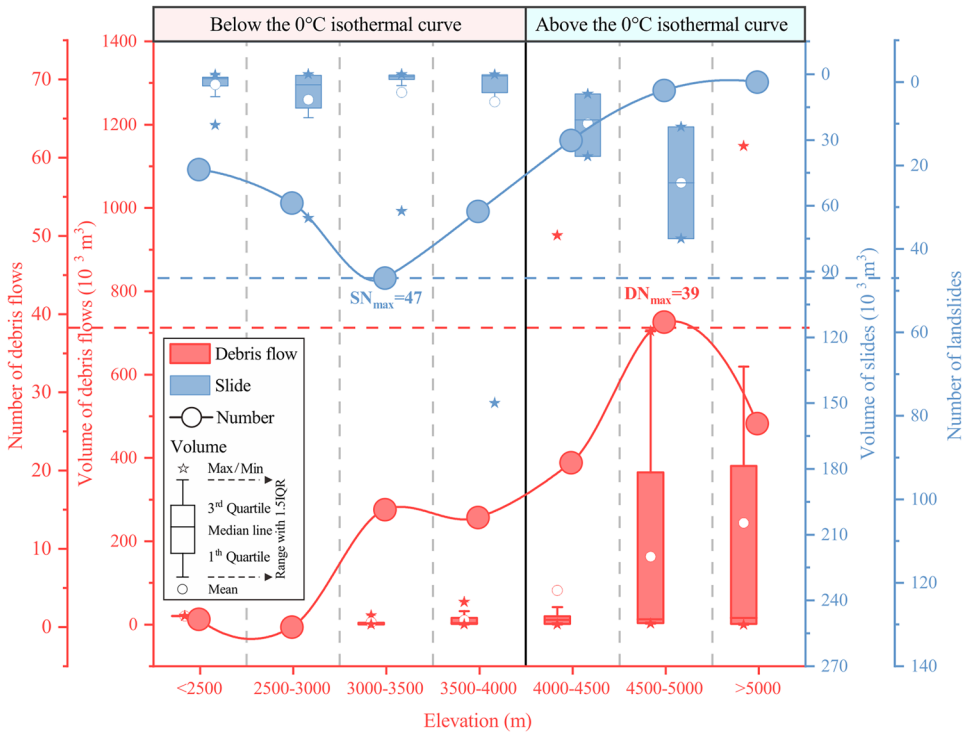

Fig. 10 Distribution of slides and debris flows within the different elevation intervals. DN_{max} represents the maximum number of debris flows, and SN_{max} represents the maximum number of slides

rainfall-induced landslides are likely to occur frequently under scenario SSP2.6 during 2020–2049. Between 2050 and 2100, the climate of the region is projected to be dry. This is attributed to the decreasing rainfall trend under all of the scenarios (except for the rainfall trend under scenario SSP 8.5 between 2050 and 2079).

The trend of snowfall differs between the scenarios (Fig. 13g–i). The snowfall trend will only be positive during 2050–2100 under scenario SSP2.6 and during 2020–2049 under scenario SSP4.5. Additionally, the snowfall trend will be greater in the region above the 0 °C isotherm curve than in the region below the 0 °C isotherms. This indicates that under this scenario and during this time period, there will be more large-sized debris flows in the region above the 0 °C isotherm curve.

We inferred the anticipated changes in the landslides in this region (Fig. 14) based on the above results (the "Distribution of landslides with elevation" and "Landslides with climate change-elevation relationship" sections) for the triggering factors and distribution trends (including the volume and number) of the landslides within the different elevation intervals, as well as the predicted climate change in the different scenarios, periods, and elevation intervals (Fig. 13). Between 2020 and 2049, we expect more and larger debris flows to occur in the area above the 0 °C isotherm curve. This is because the increase in temperature trend with elevation will intensify the snowmelt, glacier retreat, and permafrost degradation in this region, thus increasing the occurrence of debris flows in the area above the 0 °C isotherm curve. Especially under scenario SSP4.5, the positive snowfall trend will supplement the hydrodynamic source for the occurrence of debris flows. Moreover, the areas below the 0 °C isotherms will see an increase in small-volume slides. This is due to the possibility that a positive rainfall trend could exacerbate the occurrence of torrential rainfall, which would induce slides in the area below the 0 °C isotherm curve. Between 2050 and 2079, some large-volume debris flows could develop in the region above the 0 °C isotherm curve. This is due to the fact that the increase in temperature trend with elevation will accelerate the snowmelt, glacier retreat, and permafrost degradation, which will increase the occurrence of debris flows in the area above the 0 °C isotherm curve. In particular, favorable snowfall and rainfall trends would enhance the hydrodynamic sources for the occurrence of debris flows in the area above the 0 °C isotherms under scenarios SSP 2.6 and SSP 8.5. During this period, slides are only likely to occur in the areas below the 0 °C isotherm curve under scenario SSP8.5. From 2080 to 2100, some debris flows are expected to occur in the region above the 0 °C isotherms, and in this region only, under scenario SSP2.6.

Discussion

Response of landslide activity to climate change

In Taxkorgan County, there is a lack of a long time series (> 20 years) of landslide inventories and a set of meteorological data that can reflect climate change at high elevations, which has caused the numerous studies on landslides in this region that have focused on analyzing the spatial susceptibility and conducting a qualitative analysis of the stability of individual slopes and landslides (Schneider 2004; Jiang et al. 2021). In this study, we reconstructed the landslide inventory over the past 20 years, quantified the relationship between landslides and climate change within the different elevation intervals, revealed the key factors of landslide-inducing, and predicted the future development of landslides within

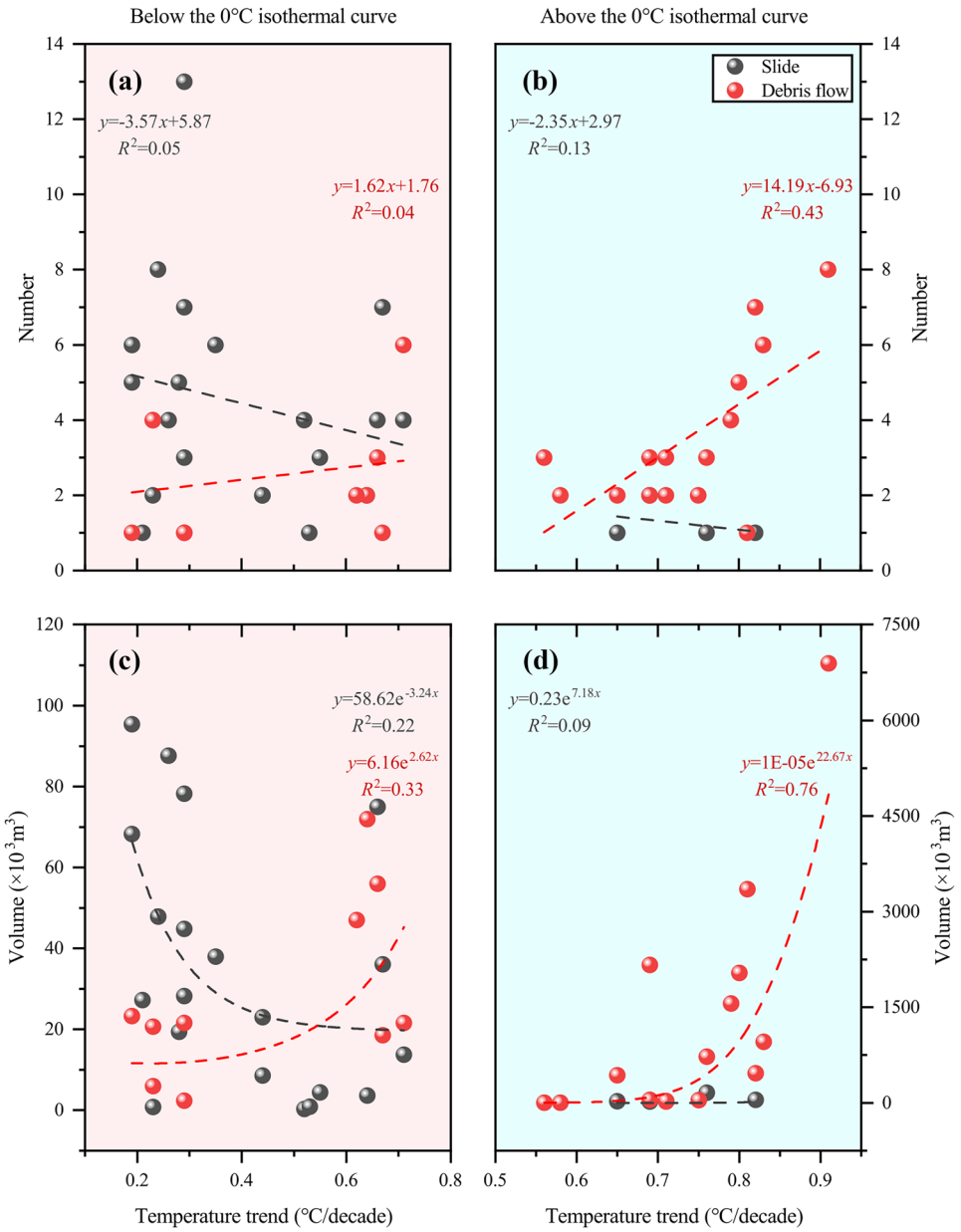

Fig. 11 The triggering factors of the slides and debris flows. **a**, **c** The relationship between the landslide and temperature trends in the areas below the 0 °C isothermal curve. **b**, **d** The relationship between the landslide and temperature trends in the areas above the 0 °C isothermal curve. Here, the term temperature trend refers to the warming rate of the T_{max} within the different elevation intervals over the past 20 years (2000–2019)

the different elevation intervals. The results regarding the elevation dependence of landslide activity are consistent with those of previous studies (Huggel et al. 2012; Chiarle et al. 2015; Ravanel and Deline 2011; Paranunzio et al. 2016; Patton et al. 2019). The torrential rainfall-induced small-sized slides and debris flows are concentrated in areas below the 0 °C isotherm curve, which is attributed to an increase in the westerly index (WI) leading to enhanced warming and humid airflow from the North Atlantic and the Caspian Sea (Schär et al. 1996; Dai and Wang 2010; Yao et al. 2015). This in turn increases the water vapor transport and intensifies the frequency of rainfall-induced slides in low mountain areas. In the areas above the 0 °C isotherm curve, large-sized debris flows induced by glacial retreat, snowmelt, and permafrost degradation are dominant. In particular, large-sized landslides increase exponentially with increasing temperature trends in alpine regions covered by glacial erosion and ice denudation landforms. This is because in the areas above the 0 °C isotherm curve, elevation-dependent warming and wetting (Yan and Liu 2014) result in accelerated local water circulation, exacerbated summer glacier/snow cover melting, and permafrost degradation, resulting in slope instability, which further contributes to the formation of large-sized landslides in high mountain areas (Seneviratne 2012).

Furthermore, our findings show that a large number of landslides does not necessarily indicate a higher landslide hazard in the region because these are the smallest landslides (Fig. 10). In Taxkorgan County, 46.1% of the small-sized rock landslides (17 debris flows and 102 slides) are distributed in low-elevation areas (elevations of < 4000 m); that is, in areas below the 0 °C isothermal

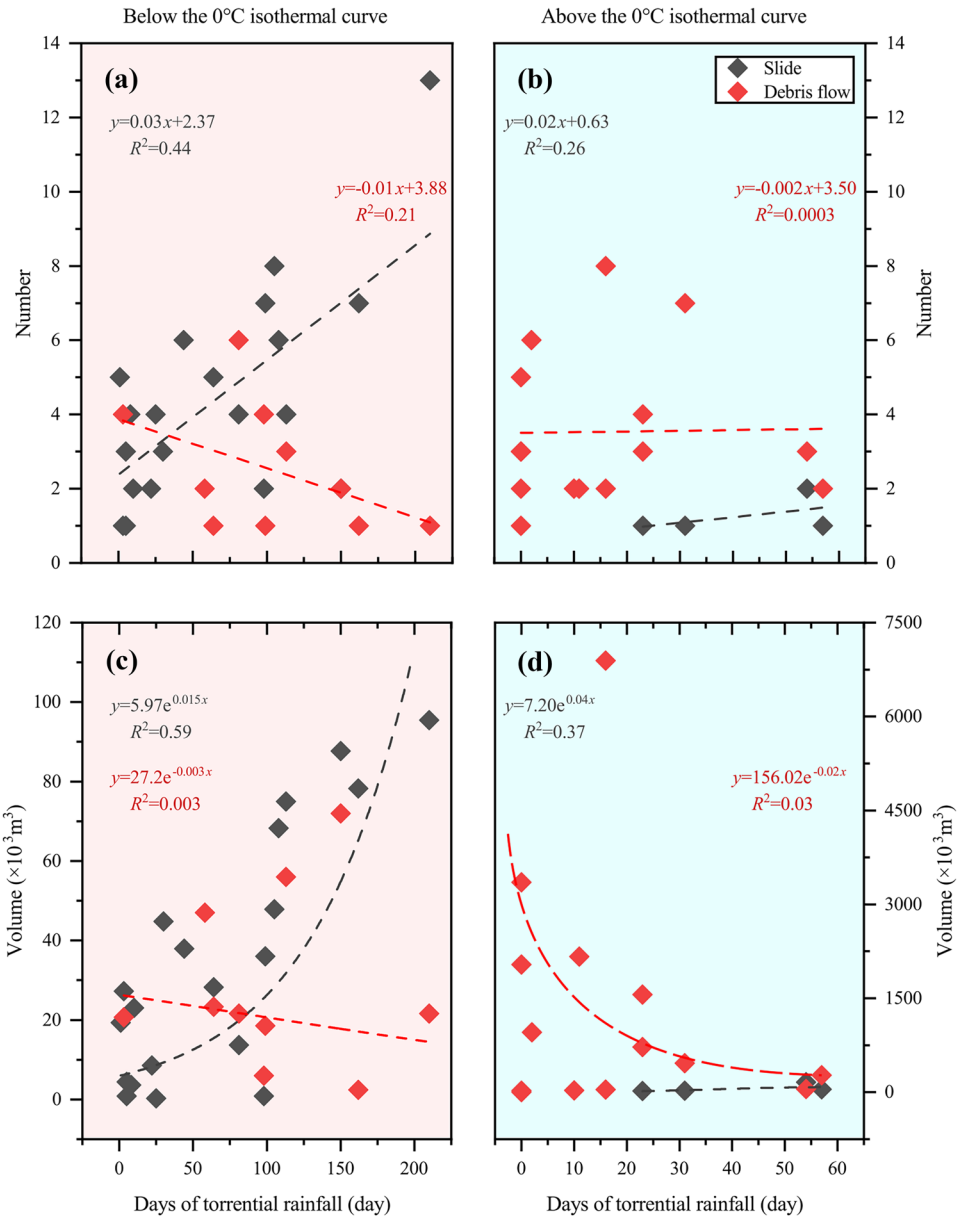

Fig. 12 The effect of torrential rainfall on the slides and debris flows. **a**, **c** The relationship between the landslides and torrential rainfall in the areas below the 0 °C isothermal curve. **b**, **d** The relationship between the landslides and torrential rainfall in the areas above the 0 °C isothermal curve. Notably, the number of days of torrential rainfall refers to the number of days with a 24-h rainfall of greater than 24 mm within the different elevation intervals over the past 20 years (2000–2019)

curves (Fig. 2). In areas below the 0 °C isothermal curve (< 3500 m), slides and debris flows appear to be becoming more frequent, and the number of slides and debris flows peaks within an interval of 3000–3500 m. However, the volume within the 3000–3500 m interval is the smallest (Fig. 10). Thus, we believe that a large number of landslides does not necessarily indicate a higher landslide hazard in this region. We should place more emphasis on the large volume of landslides caused by snow melt, glacier retreat, and glacier fracturing that occur above the 0 °C isotherms, where the hazard may be more severe. Typical examples are the glacial debris flows that occurred in Bulunkou Township (Jiang et al. 2012), the slide induced by snowmelt in Taheman Township (Seong et al. 2009; Yuan et al. 2013) in the Pamirs, and the catastrophic landslide that occurred in Chamoli, India, in the southern hills of the Himalayas on February 7, 2021 (Jiang et al. 2021), all of which caused significant damage to human lives and property. Due to the lack of a climate and landslide observation network at high elevations, the occurrence of large landslides caused by climate change cannot be accurately monitored in a timely fashion allowing for sufficient warning, resulting in losses (Yao et al. 2019, 2022; Zou et al. 2020). Based on the elevation dependence of landslide activity, we propose the integration of an observational network composed of surface in-situ climate observations in the high-elevation intervals, satellite data, and high-resolution climatic modeling to increase our understanding of the elevation dependence of landslide activity in other alpine regions.

Behavior of 0 °C isotherm curve

The elevation of the 0 °C isotherm curve in Taxkorgan County has increased significantly over the past 20 years (i.e., it has moved up

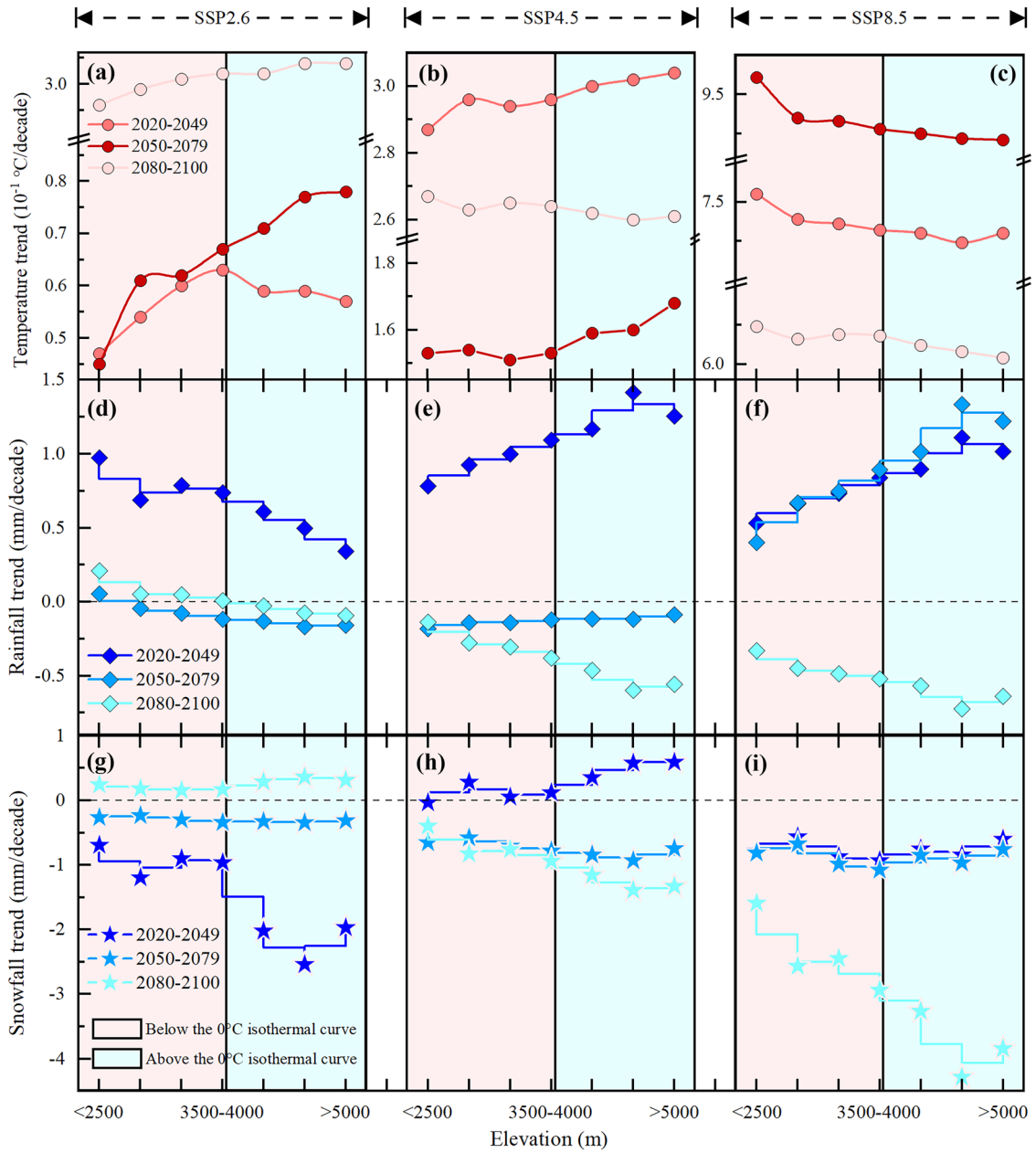

Fig. 13 Predicted climate trends within the different elevation intervals under different climate scenarios. **a**–**c** Future warming rates. **d**–**f** Future rainfall trends. **g**–**i** Future snowfall trends. Note: The two black dashed lines on the graph denote the 0 values of the rainfall and snowfall trends

186.38 m), and the average elevation of the 0 °C isotherm curve in the warm season (May–September over the past 20 years) was 4061.196 m. The significant upward shift of the 0 °C isotherms in the northern part (in the Pamirs) of the study area indicates that the 0 °C isotherm moves upward as the temperature increase under global warming, which in turn indicates that Taxkorgan County is an area sensitive to climate change. However, in the southeastern part (in the Karakoram) of the study area, the 0 °C isotherms exhibited a trend or a small downward shift (Fig. 2). Previous works have shown that the masses of the glaciers nourished by winter-westerly precipitation in the Karakorum region have remained stable or have small gains (Hewitt 2005; Gardelle et al. 2013; Rankl and Braun 2016; Berthier and Brun 2019), causing the 0 °C isotherms of the region to tend to be stable or to shift downward. Moreover, the climate change (temperature, annual precipitation) observed via ground-based weather stations may not necessarily be representative of the high-elevation areas (Hassan et al. 2017; Hewitt 2007). In order to produce meteorological data that can reflect climate change at high elevations, in this study, we downscaled the GLDAS dataset based on ground-based weather station observations and a DEM. We found that there was an increase in the precipitation trend of the area above the 0 °C isotherms (Fig. 9c), which helped to increase the

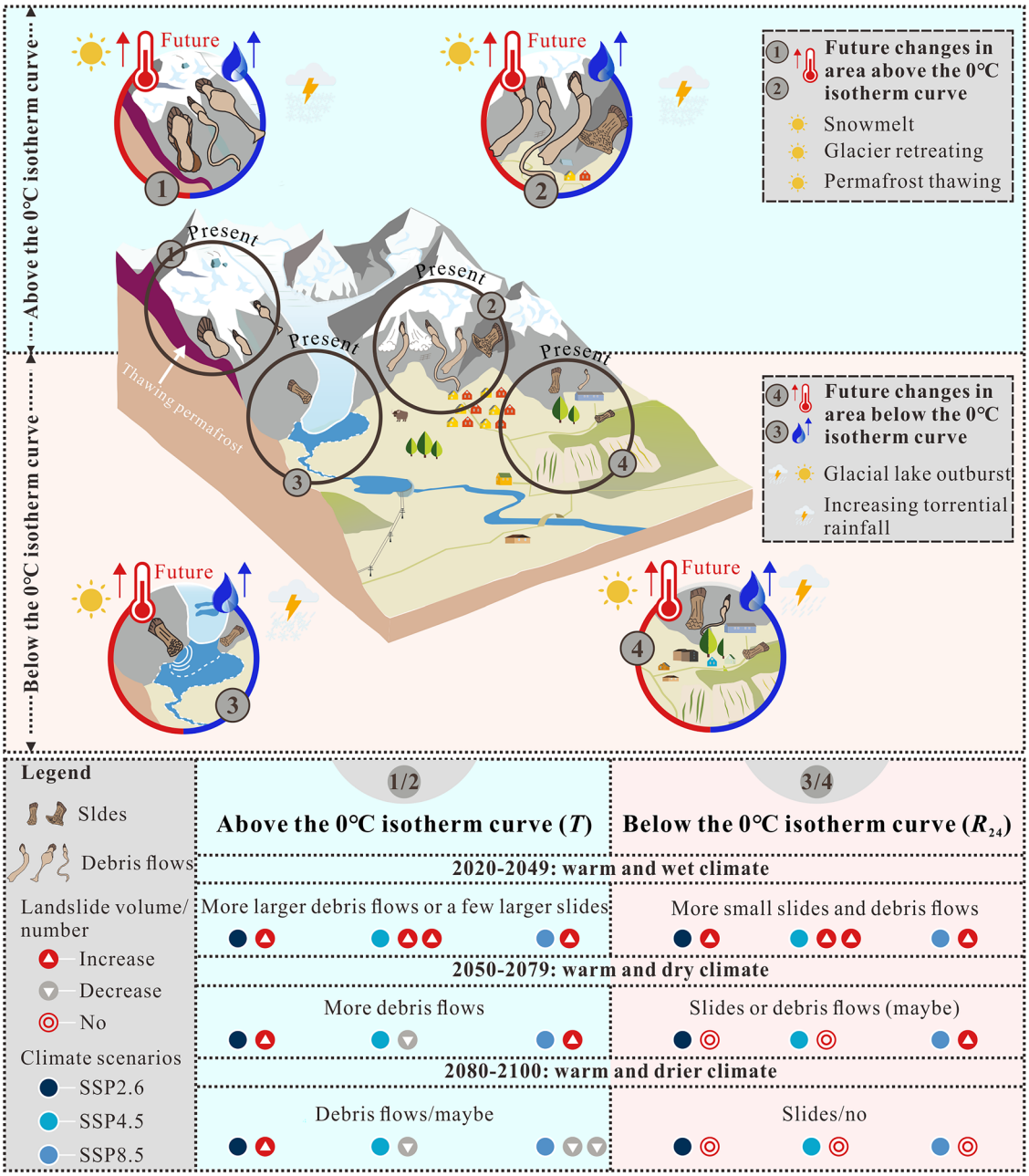

Fig. 14 Schematic diagram of the changes in the landslides in the areas below and above the 0 °C isotherm curve in the future (revised by Hock et al. (2019)). The red thermometer and the blue raindrops are used to express future changes in temperature and precipitation (rainfall and snowfall) in this region. Numbers 1, 2, 3, and 4 are the scenarios we selected to show the present and future landslides within the different elevation intervals (landform types). Number 1 is a scenario of landslides in the alpine areas (elevation > 4500 m), 2 and 3 are scenarios of landslides in the mid-alpine areas (3500–4500 m), and 4 is a scenario of landslides in the valleys (elevation < 3500 m). "No" indicates that no slides or debris flows will occur in the area at some point in the future. An increasing or decreasing symbol denotes an increase or decrease in the number/volume of landslides, while two symbols indicate a greater increase or decrease. "Maybe" indicates the possibility of an increase, decrease, or absence of the landslides

precipitation (snowfall) in this area and thus to increase the glacier mass and snow cover area. This caused the o °C isotherms in the southeastern part of Taxkorgan County to remain stable or shift upward. This result is consistent with previous studies (Minora et al. 2013; Bashir et al. 2017).

Conclusions

In this study, we took Taxkorgan County in the eastern Pamirs as the study area to investigate the elevation dependence of landslide activity induced by climate change based on a historical landslide inventory and downscaling of climatic data. Over the past

20 years, the number and volume of inventoried shallow landslides in the area have increased due to climate change. The temperature and precipitation trends in the area have exhibited strong elevation dependence, and the number of days of torrential rainfall has gradually increased in the region below the 0 °C isotherm curve. The small-sized ($< 50 \times 10^3$ m^3) slides caused by torrential rainfall have been concentrated in the region below the 0 °C isotherm curve. In contrast, large-volume ($> 50 \times 10^3$ m^3) debris flows induced by maximum temperature have mainly occurred in the areas above the 0 °C isotherm curve and have exhibited a strong elevation dependence. In the future (2020–2049), more small-sized landslides will occur below the 0 °C isotherm curve as the climate continues to become warmer and wetter. The number and volume of the large-sized debris flow in the regions above the 0 °C isotherm curve will continuously increase. Based on the elevation-dependence of landslide activity, we propose the integration of the observational network of surface in-situ climate observations in high-elevation intervals, satellite data, and high-resolution climatic modeling to increase our understanding of the elevation-dependence of landslide activity in other alpine regions. Such information would provide a basis for better disaster risk assessment and management.

Acknowledgements

This work was funded by the International Science and Technology Cooperation Program of China (Grant No. 2018YFE0100100), The Second Tibetan Plateau Scientific Expedition and Research Program (STEP) (Grant No. 2019QZKK0902), National Natural Science Foundation of China (Grant No. 42271078) and Natural Science Basic Research Program of Shaanxi (Grant No. 2021JC-40). We would also like to thank Engineer Zhiyuang Feng from the Administration of Natural Resources of Kashgar for his assistance in the fieldwork.

Declarations

Conflict of interest The authors declare no competing interests.

References

Allen SK, Rastner P, Arora M, Huggel C, Stoffel M (2016) Lake outburst and debris flow disaster at Kedarnath, June 2013: hydrometeorological triggering and topographic predisposition. Landslides 13:1479–1491. https://doi.org/10.1007/s10346-015-0584-3

Bashir F, Zeng X, Gupta H, Pieter H (2017) A hydrometeorological perspective on the Karakoram anomaly using unique valley-based synoptic weather observations. Geophys Res Lett 44(20):470–478. https://doi.org/10.1002/2017GL075284

Berthier´E, Brun F (2019) Karakoram geodetic glacier mass balances between 2008 and 2016: persistence of the anomaly and influence of a large rock avalanche on Siachen Glacier. J Glaciol 65(251):494–507. https://doi.org/10.1017/jog.2019.32

Carrara A, Crosta G, Frattini P (2003) Geomorphological and historical data in assessing landslide hazard. Earth Surf Proc Land 28(10):1125–1142. https://doi.org/10.1002/esp.545

Chai MT, Mu YH, Zhang JM, Ma W (2018) Characteristics of asphalt pavement damage in degrading permafrost regions: case study of the Qinghai-Tibet Highway. China J Cold Reg Eng 32(2):05018003. https://doi.org/10.1061/(ASCE)CR.1943-5495.0000165

Chiarle M, Coviello V, Arattano M, Silvestri P, Nigrelli G (2015) High elevation rock falls and their climatic control: a case study in the Conca di Cervinia (NW Italian Alps). Eng Geol Soc Territory 1:439–442. https://doi.org/10.1007/978-3-319-09300-0_84

Coe JA (2012) Regional moisture balance control of landslide motion: implications for landslide forecasting in a changing climate. Geology 40(4):323–326. https://doi.org/10.1130/G32897.1

Coe JA, Godt JW (2012) Review of approaches for assessing the impact of climate change on landslide hazards. Taylor & Francis Group London pp:371–377

Coe JA, Bessette-Kirton EK, Geertsema M (2018) Increasing rock avalanche size and mobility in Glacier Bay National Park and Preserve, Alaska detected from 1984–2016 Landsat imagery. Landslides 15:393–407. https://doi.org/10.1007/s10346-017-0879-7

Coe JA (2020) Bellwether sites for evaluating changes in landslide frequency and magnitude in cryospheric mountainous terrain: a call for systematic, long-term observations to decipher the impact of climate change. Landslides 17(11):2483–2501. https://doi.org/10.1007/10346-020-01462-y

Cody E, Draebing D, McColl S, Brideau M (2020) Geomorphology and geological controls on an active paraglacial rockslide in the New Zealand Southern Alps. Landslides 17:755–776. https://doi.org/10.1007/s10346-019-01316-2

Cruden DM, Varnes DJ (1996) Landslide types and processes. In: Turner AK, Schuster RL (Eds.), Landslides: investigation and mitigation. Special-Report 247, Transportation Research Board, National Research Council. National Academy Press, Washington, DC pp:36–75

Dai XG, Wang P (2010) Zonal mean mode of global warming over the past 50 years. Atmos Ocean Sci Lett 3(1):45–50. https://doi.org/10.1080/16742834.2010.11446835

Deng YH, Wang SJ, Bai XY, Wu LH, Cao Y, Li HW, Wang MM, Li CJ, Yang YJ, Hu ZY, Tian SQ, Lu Q (2020) Comparison of soil moisture products from microwave remote sensing, land model, and reanalysis using global ground observations. Hydrol Process 34(3):1–47. https://doi.org/10.1002/hyp.13636

Diaz-Nieto J, Wilby RL (2005) A comparison of statistical downscaling and climate change factor methods: impacts on low flows in the river Thames. United Kingdom Climatic Change 69(2–3):245–268. https://doi.org/10.1007/s10584-005-1157-6

Eriksen HO, Rouyet L, Lauknes TR, Berthling I, Isaksen K, Hindberg H, Larsen Y, Corner GD (2018) Recent acceleration of a rock glacier complex, Ádjet, Norway, documented by 62 years of remote sensing observations. Geophys Res Lett 45(16):8314–8323. https://doi.org/10.1029/2018GL077605

Fatolazadeh F, Eshagh M, Gota K (2020) A new approach for generating optimal GLDAS hydrological products and uncertainties. Sci Total Environ 737:138932. https://doi.org/10.1016/j.scitotenv.2020.138932

Firozjaei MK, Fathololoumi S, Panah S, Kiavarz M, Biswas A (2020) A new approach for modeling near surface temperature lapse rate based on normalized land surface temperature data. Remote Sens Environ 242:1–20. https://doi.org/10.1016/j.rse.2020.111746

Fujita K, Sakai A, Takenaka S, Nuimura T, Yamanokuchi T (2013) Potential flood volume of Himalayan glacial lakes. Nat Hazards Earth Syst Sci Discuss 1(1):1827–1839. https://doi.org/10.5194/nhessd-1-15-2013

Gardelle J, Berthier E, Arnaud Y, Kaab A (2013) Region-wide glacier mass balances over the Pamir-Karakoram-Himalaya during 1999–2011. Cryosphere 7:1263–1286. https://doi.org/10.5194/tc-7-1885-2013

Grose MR, Narsey S, Delage F, Dowdy AJ, Power SB (2020) Insights from CMIP6 for Australia's future climate. Earth's Future 8(5):480–504. https://doi.org/10.1002/essoar.10501525.1

Guzzetti F, Cardinali M, Reichenbach P, Carrara A (2000) Comparing landslide maps: a case study in the upper Tiber River Basin, central Italy. Environ Manage 25(3):247–363. https://doi.org/10.1007/s002679910020

Guzzetti F, Mondini AC, Cardinali M, Fiorucci F, Santangelo M, Chang KT (2012) Landslide inventory maps: new tools for an old problem. Earth Sci Rev 112(1–2):42–66. https://doi.org/10.1016/j.earscirev.2012.02.001

Haeberli W, Whiteman C (2015) Snow and ice-related hazards, risks, and disasters. Elsevier, Amsterdam 812. https://doi.org/10.1016/B978-0-12-817129-5.00014-7

Harrison S, Kargel JS, Huggel C, Reynolds JM, Vilímek V (2018) Climate change and the global pattern of moraine-dammed glacial lake outburst floods. Cryosphere 12(4):1195–1209. https://doi.org/10.5194/tc-12-1195-2018

Hassan J, Kayastha RB, Shrestha A, Bano I, Ali SH, Magsi HZ (2017) Predictions of future hydrological conditions and contribution of snow and ice melt in total discharge of Shigar River Basin in Central Karakoram. Pakistan. Sci Cold Arid Reg 9(6):511–524

Hay LE, Wilby RL, Leavesley GH (2010) A comparison of Delta change and downscaled GCM scenarios for three mountainous basins in the United States. J Am Water Resour Assoc 36(2):387–397. https://doi.org/10.1111/j.1752-1688.2000.tb04276.x

Hewitt K (2005) The Karakoram anomaly? Glacier expansion and the 'elevation effect.' Karakoram Himalaya Mountain Research and Development 25(4):332–341. https://doi.org/10.1659/0276-4741(2005)025[0332:TKAGEA]2.0.CO;2

Hewitt K (2007) Tributary glacier surges: an exceptional concentration at Panmah Glacier. Karakoram Himalaya International Glaciological Society 53(181):181–188. https://doi.org/10.3189/172756507782202829

Hewitt K (2009) Rock avalanches that travel onto glaciers and related developments, Karakoram Himalaya. Inner Asia Geomorphology 103(1):66–79. https://doi.org/10.1016/j.geomorph.2007.10.017

Hock R, Rasul G, Adler C, Cáceres B, Gruber S, Hirabayashi Y, Jackson M, Kääb A, Kang S, Kutuzov S, Milner A, Molau U, Morin S, Orlove B, Steltzer H (2019) High mountain areas. In: IPCC Special Report on the Ocean and Cryosphere in a Changing Climate. In press

Hu YY, Xu Y, Li JJ, Han ZY (2021) Evaluation on the performance of CMIP6 global climate models with different horizontal resolution in simulating the precipitation over China. Clim Change Res 2:1–19

Huggel C, Clague JJ, Korup O (2012) Is climate change responsible for changing landslide activity in high mountains? Earth Surf Proc Land 37(1):77–91. https://doi.org/10.1002/esp.2223

Hungr O, Leroueil S, Picarelli L (2014) The Varnes classification of landslide types, an update. Landslides 11(2):167–194. https://doi.org/10.1007/s10346-013-0436-y

Jakob M, Owen T (2021) Projected effects of climate change on shallow landslides, North Shore Mountains, Vancouver, Canada. Geomorphology 25:1–16. https://doi.org/10.1016/j.geomorph.2021.107921

Jiang N, Su F, Li Y, Guo X, Liu X (2012) Debris flow assessment in the Gaizi-Bulunkou section of Karakoram Highway. Front Earth Sci 9:660579. https://doi.org/10.3389/feart.2021.660579

Jiang Q, Chan D, Xiong J (2016) Back analysis of a debris landslide based on real-time video record: sliding process and post-sliding investigation. Bull Eng Geol Environ 75(2):647–658. https://doi.org/10.1007/s10064-015-0831-9

Jiang R, Zhang L, Peng D, He X, He J (2021) The landslide hazard chain in the Tapovan of the Himalayas on 7 February 2021. Geophys Res Lett 48:1–11. https://doi.org/10.1029/2021GL093723

Kang ZW, Zhang ZY, Liu L, Wang TX, Tian H, Chen HJ, Zhang XY (2022) Spatio-temporal variation characteristics of land surface temperature in Xinjiang based on MODIS. Geogr Res 41(04):997–1017. https://doi.org/10.11821/dlyj020210232

Key JR, Collins JB, Fowler C, Stone RS (1997) High-latitude surface temperature estimates from thermal satellite data. Remote Sens Environ 61(2):302–309. https://doi.org/10.1016/S0034-4257(97)89497-7

Khadka D, Babel MS, Shrestha S, Tripathi NK (2014) Climate change impacts on glacier and snowmelt and runoff in the Tamakoshi basin in the Hindu Kush Himalayan (HKH) region. J Hydrol 511:49–60. https://doi.org/10.1016/j.jhydrol.2014.01.005

Kirschbaum DB, Adler R, Hong Y, Hill S, Lerner-Lam A (2010) A global landslide catalog for hazard applications: method, results, and limitations. Nat Hazards 52(3):561–575. https://doi.org/10.1007/s11069-009-9401-4

Kirschbaum D, Kapnick SB, Stanley T, Pascale S (2020) Changes in extreme precipitation and landslides over high mountain Asia. Geophys Res Lett 47(4):1–9. https://doi.org/10.1029/2019GL085347

Li JL, Chen X, Bao AM, Shen ZF, Ji SP (2016a) Glacier hazard emergency monitoring of the Jiubie Peak in Kongur Mountains using unmanned aerial vehicle photogrammetry. Arid Land Geography 39(2):378–386

Li BF, Chen YN, Chen ZS, Xiong HG, Lian LS (2016b) Why does precipitation in northwest China show a significant increasing trend from 1960 to 2010? Atmos Res 167:275–284. https://doi.org/10.1016/j.atmosres.2015.08.017

Liu Y, Yang Z, Lin P, Zheng Z, Xie S (2019) Comparison and evaluation of multiple land surface products for the water budget in the yellow river basin. J Hydrol 584:1–59. https://doi.org/10.1016/j.jhydrol.2019.124534

Liu ZJ, Qiu HJ, Zhu YR, Liu Y, Yang DD, Ma SY, Zhang JJ, Wang YY, Wang LY, Tang BZ (2022) Efficient identification and monitoring of landslides by time-series InSAR combining single- and multi-look phases. Remote Sens 14(4):1026. https://doi.org/10.3390/rs14041026

Liu ZJ, Qiu HJ, Ma SY, Yang DD, Pei YQ, Du C, Sun HS, Hu S, Zhu YR (2021) Surface displacement and topographic change analysis of the Changhe landslide on September 14, 2019. China Landslides 18(4):1471–1483. https://doi.org/10.1007/s10346-021-01626-4

Ma XJ, Hao YG, Wang YX, Zhou XY, Li B, Juma TEX, Shi J, Pan S, Han FF, Han QY (2016) Detailed investigation report on geo-hazards in Taxkorgan County, Xinjiang. National Geological Data Library. https://doi.org/10.35080/n01.c.172136

Ma F, Yuan X, Jiao Y, Ji P (2020) Unprecedented Europe heat in June-July 2019: risk in the historical and future context. Geophys Res Lett 47(11):e2020GL087809. https://doi.org/10.1029/2020GL087809

Ma SY, Qiu HJ, Zhu YR, Yang DD, Tang BZ, Wang DZ, Wang LY, Cao MM (2023) Topographic changes, surface deformation and movement process before, during and after a Rotational Landslide. Remote Sens 15:662. https://doi.org/10.3390/rs15030662

Minora U, Bocchiola D, Agata C, Maragno D, Mayer C, Lambrecht A, Mosconi B, Vuillermoz E, Senese A, Compostella C (2013) 2001–2010 glacier changes in the Central Karakoram National Park: a contribution to evaluate the magnitude and rate of the "Karakoram anomaly." The Cryosphere Discussions 7(3):2891–2941. https://doi.org/10.5194/tcd-7-2891-2013

Miralles DG, Teuling AJ, Heerwaarden CCV, Arellano JVD (2014) Megaheatwave temperatures due to combined soil desiccation and atmospheric heat accumulation. Nat Geosci 7:345–349. https://doi.org/10.1038/ngeo2141

Ni J, Wu T, Zhu X, Hu G, Yang C (2020) Simulation of the present and future projection of permafrost on the Qinghai-Tibet Plateau with statistical and machine learning models. J Gerontol Ser A Biol Med Sci 126(2):1–20. https://doi.org/10.1002/essoar.10503593.2

Nie Y, Sheng YW, Liu Q, Liu L, Liu S, Zhang Y, Song C (2017) A regional-scale assessment of Himalayan glacial lake changes using satellite observations from 1990 to 2015. Remote Sens Environ 189:1–13. https://doi.org/10.1016/j.rse.2016.11.008

Ohmura A (2012) Enhanced temperature variability in high-altitude climate change. Theoret Appl Climatol 110(4):499–508. https://doi.org/10.1007/s00704-012-0687-x

Panagos P, Ballabio C, Meusburger K, Spinoni J, Alewell C, Borrelli P (2017) Towards estimates of future rainfall erosivity in Europe based on redes and worldclim datasets. J Hydrol 548:251–262. https://doi.org/10.1016/j.jhydrol.2017.03.006

Paranunzio R, Laio F, Chiarle M, Nigrelli G, Guzzetti F (2016) Climate anomalies associated to the occurrence of rockfalls at high-elevation in the Italian Alps. Nat Hazards Earth Syst Sci 16(9):2085–2106. https://doi.org/10.5194/nhess-2016-100

Patton AI, Rathburn SL, Capps DM (2019) Landslide response to climate change in permafrost regions. Geomorphology 340:116–128. https://doi.org/10.1016/j.geomorph.2019.04.029

Pei YQ, Qiu HJ, Yang DD, Liu ZJ, Ma SY, Li JY, Cao MM, Waili WFE (2023) Increasing landslide activity in the Taxkorgan River Basin (eastern Pamirs Plateau, China) driven by climate change. CATENA 223:106911. https://doi.org/10.1016/j.catena.2023.106911

Pepin N, Bradley RS, Diaz HF, Baraer M, Caceres EB, Forsythe N, Fowler H, Greenwood G, Hashmi MZ, Liu XD, Miller JR, Ning L, Ohmura A, Palazzi E, Rangwala I, Schöner W, Severskiy I, Shahgedanova M, Wang MB, Williamson SN, Yang DQ (2015) Elevation-dependent warming in mountain regions of the world. Nat Clim Chang 5(5):424–430. https://doi.org/10.1038/NCLIMATE2563

Petley DN (2012) The Siachen Glacier avalanche (138 people killed) was an ice-rock avalanche. https://blogs.agu.org/landslideblog/2012/04/12/the-Siachen-glacier-avalanche-135-people-killed-was-actually-alandslide/

Piacentini D, Troiani F, Daniele G, Pizziolo M (2018) Historical geospatial database for landslide analysis: the Catalogue of Landslide Occurrences in the Emilia-Romagna Region (CLOCKER). Landslides 15(4):811–822. https://doi.org/10.1007/s10346-018-0962-8
Qi W, Liu JG, Yang H, Zhu XP, Tian Y, Jiang X, Huang X, Feng L (2020) Large uncertainties in runoff estimations of GLDAS versions 2.0 and 2.1 in China. Earth Space Sci 7(1):1–29. https://doi.org/10.1029/2019EA000829
Qiu HJ, Zhu YR, Zhou WQ, Sun HS, He JY, Liu ZJ (2022) Influence of DEM resolution on landslide simulation performance based on the Scoops3D model. Geomat Nat Haz Risk 13(1):1663–1681. https://doi.org/10.1080/19475705.2022.2097451
Rankl M, Braun M (2016) Glacier elevation and mass changes over the Central Karakoram region estimated from TanDEM-X and SRTM/X-SAR digital elevation models. Ann Glaciol 57(71):273–281. https://doi.org/10.3189/2016AoG71A024
Ravanel L, Deline P (2011) Climate influence on rockfalls in high-Alpine steep rockwalls: the north side of the Aiguilles de Chamonix (Mont Blanc massif) since the end of the 'Little Ice Age.' Holocene 21(2):357–365. https://doi.org/10.1177/0959683610374887
Rgi C, Nosenko G (2017) Randolph Glacier Inventory (RGI)-A dataset of global glacier outlines: version6.0. Technical Report, Global Land Ice Measurements from Space
Robinson AC, Yin A, Manning CE, Harrison TM, Zhang SH, Wang XF (2007) Cenozoic evolution of the eastern Pamir: implications for strain-accommodation mechanisms at the western end of the Himalayan-Tibetan orogen. Geol Soc Am Bull 119(7–8):882–896. https://doi.org/10.1130/B25981.1
Rolland C (2003) Spatial and seasonal variations of air temperature lapse rates in Alpine regions. J Clim 16(7):1032–1046. https://doi.org/10.1175/1520-0442(2003)016%3c1032:SASVOA%3e2.0.CO;2
Rossi M, Witt A, Guzzetti F, Malamud BD, Peruccacci S (2010) Analysis of historical landslide time series in the Emilia-Romagna region, northern Italy. Earth Surf Proc Land 35(10):1123–1137. https://doi.org/10.1002/esp.1858
Schär C, Frei C, Lüthi D, Davies HC (1996) Surrogate climate change scenarios for regional climate models. Geophys Res Lett 23(6):669–672. https://doi.org/10.1029/96GL00265
Schneider JF (2004) Risk assessment of remote geohazards in central and southern Pamir, Tajikistan. Workshop, Bishkek Kyrgyzstan, pp:164–169
Schulz J, Albert P, Behr HD, Caprion D, Zelenka A (2008) Operational climate monitoring from space: the EUMETSAT Satellite Application Facility on Climate Monitoring (CM-SAF). Atmos Chem Phys 9(5):1687–1709. https://doi.org/10.5194/acpd-8-8517-2008
Seneviratne SI (2012) Changes in climate extremes and their impacts on the natural physical environment. Cambridge University Press pp:109–230. https://doi.org/10.1017/CBO9781139177245.006
Seong YB, Owen LA, Yi C, Finkel RC, Schoenbohm L (2009) Geomorphology of anomalously high glaciated mountains at the northwestern end of Tibet: Muztag Ata and Kongur Shan. Geomorphology 103(2):227–250. https://doi.org/10.1016/j.geomorph.2008.04.025
Shi XH, Xu XD (2008) Interdecadal trend turning of global terrestrial temperature and precipitation during 1951–2002. Prog Nat Sci-Mater Int 18(11):1383–1393. https://doi.org/10.1016/j.pnsc.2008.06.002
Tanyaş H, Van Westen CJ, Allstadt KE, Jessee MAN, Görüm T, Jibson RW, Godt JW, Sato HP, Schmitt RG, Marc O, Hovius N (2017) Presentation and analysis of a worldwide database of earthquake-induced landslide inventories. J Geophys Res Earth Surf 122(10):1991–2015. https://doi.org/10.1002/2017JF004236
Veh G, Korup O, Walz A (2020) Hazard from Himalayan glacier lake outburst floods. Proc Natl Acad Sci 117(2):907–912. https://doi.org/10.1073/pnas.1914898117
Wang LY, Qiu HJ, Zhou WQ, Zhu YR, Liu ZJ, Ma SY, Yang DD, Tang BZ (2022) The post-failure spatiotemporal deformation of certain translational landslides may follow the pre-failure pattern. Remote Sens 14(10):2333. https://doi.org/10.3390/rs14102333
Wirz V, Geertsema M, Gruber S, Purves RS (2016) Temporal variability of diverse mountain permafrost slope movements derived from multi-year daily GPS data, Mattertal. Switzerland Landslides 13(1):67–83. https://doi.org/10.1007/s10346-014-0544-3
Yan L, Liu X (2014) Has climatic warming over the Tibetan Plateau paused or continued in recent years? Earth Ocean Atmos Sci 1:13–28
Yao J, Chen Y, Guan X, Zhao Y, Chen J, Mao W (2022) Recent climate and hydrological changes in a mountain-basin system in Xinjiang, China. Earth-Sci Rev 226:1–21. https://doi.org/10.1016/j.earscirev.2022.103957
Yao JQ, Chen YN, Yang Q (2015) Spatial and temporal variability of water vapor pressure in the arid region of northwest China, during 1961–2011. Theoret Appl Climatol 123(3–4):683–691. https://doi.org/10.1007/s00704-015-1373-6
Yao JQ, Yang Q, Mao WY, Zhao Y, Xu XB (2016) Precipitation trend-elevation relationship in arid regions of China. Global Planet Change 143:1–9. https://doi.org/10.1016/j.gloplacha.2016.05.007
Yao TD, Xue YD, Chen DL, Chen FH, Thompson L, Cui P, Toshio K, Lau WKM, Lettenmaier D, Mosbrugger V, Zhang RH, Xu BQ, Dozier J, Gillespie T, Gu Y, Kang SC, Piao SL, Sugimoto S, Ueno KC, Wang L, Wang WC, Zhang F, Sheng YW, Guo WD, Ailikun YXX, Ma YM, Shen SSP, Su ZB, Chen F, Liang SL, Liu YM, SinghVP YK, Yang DQ, Zhao XQ, Qian Y, Zhang Y, Li Q (2019) Recent third pole's rapid warming accompanies cryospheric melt and water cycle intensification and interactions between monsoon and environment: multidisciplinary approach with observations, modeling, and analysis. Bull Am Meteor Soc 100(3):423–444. https://doi.org/10.1175/BAMS-D-17-0057.1
Yuan ZD, Chen J, Owen LA, Hedrick KA, Caffee MW, Li WQ, Schoenbohm LM, Robinson AC (2013) Nature and timing of large landslides within an active orogen, eastern Pamir, China. Geomorphology 182:49–65. https://doi.org/10.1016/j.geomorph.2012.10.028
Zaginaev V, Ballesteros-Canvas JA, Erokhin S, Matov E, Petrakov D, Stoffel M (2016) Reconstruction of glacial lake outburst floods in northern Tien Shan: implications for hazard assessment. Geomorphology 269:75–84. https://doi.org/10.1016/j.geomorph.2016.06.028
Zhang FY, Chen WW, Liu G, Liang SY, Kang C, He FG (2012) Relationships between landslide types and topographic attributes in a loess catchment. China J Mt Sci 9(6):742–751. https://doi.org/10.1007/s11629-012-2377-7
Zhang GQ, Yao TD, Xie HJ, Wang WC, Yang W (2015) An inventory of glacial lakes in the Third Pole region and their changes in response to global warming. Glob Planet Change 131:148–157. https://doi.org/10.1016/j.gloplacha.2015.05.013
Zhang Y, Gu J, Liu S, Wang X, Jiang Z, Wei J, Zheng Y (2022) Spatial pattern of the debris-cover effect and its role in the Hindu Kush-Pamir-Karakoram-Himalaya glaciers. J Hydrol 615:128613. https://doi.org/10.1016/j.jhydrol.2022.128613
Zhou WQ, Qiu HJ, Wang LY, Pei YQ, Tang BZ, Ma SY, Yang DD, Cao MM (2022) Combining rainfall-induced shallow landslides and subsequent debris flows for hazard chain prediction. CATENA 213:106199. https://doi.org/10.1016/j.catena.2022.106199
Zou Q, Cui P, Jiang H, Wang J, Zhou B (2020) Analysis of regional river blocking by debris flows in response to climate change. Sci Total Environ 741(7):140262. https://doi.org/10.1016/j.scitotenv.2020.140262

Yanqian Pei · Haijun Qiu (✉) · Yaru Zhu · Dongdong Yang · Bingzhe Tang · Mingming Cao
Shaanxi Key Laboratory of Earth Surface and Environmental Carrying Capacity, College of Urban and Environmental Sciences, Northwest University, Xi'an 710127, China
Email: haijunqiu@nwu.edu.cn

Yanqian Pei · Haijun Qiu · Yaru Zhu · Dongdong Yang · Bingzhe Tang · Mingming Cao
Institute of Earth Surface System and Hazards, College of Urban and Environmental Sciences, Northwest University, Xi'an 710127, China

Haijun Qiu
Email: haijunqiu@nwu.edu.cn

Jiading Wang · Fei Wang
State Key Laboratory of Continental Dynamics, Department of Geology, Northwest University, Xi'an 710069, China